Dynamics of recombination, X inactivation and centromere proteins during stick insect spermatogenesis

Zoé Dumas[1]*, William Toubiana[1]*, Marie Delattre[2], Tanja Schwander[1]

*These authors contributed equally

[1]Department of Ecology and Evolution, University of Lausanne, 1015 Lausanne.

[2]Laboratory of Biology and Modeling of the Cell, Ecole Normale Supérieure de Lyon, CNRS UMR 5239, Inserm U1293, Université Claude Bernard Lyon 1, Lyon, France.

Corresponding authors: william.toubiana@unil.ch, zoe.dumas@unil.ch.

ABSTRACT

In eukaryotes, the cellular processes contributing to gamete formation form the building blocks of genetic inheritance across generations. While traditionally viewed as conserved across model organisms, emerging studies reveal significant variation in meiotic and post-meiotic processes. Extending our knowledge to non-model organisms is therefore critical to improve our understanding of the evolutionary origin and significance of modifications associated with gamete formation. We describe the cytological patterns underlying chromosome segregation, recombination, and meiotic sex chromosome inactivation during male meiosis in the stick insect group *Timema*. Our results provide a detailed description of

24 centromere protein loading dynamics during spermatogenesis, and further reveal that 1)
25 recombination initiates before synapsis (unlike *Drosophila* meiosis), and 2) that the X remains
26 actively silenced despite two waves of transcriptional activation in autosomes during
27 spermatogenesis. Together, our observations help understand the evolutionary significance
28 of key cellular events related to spermatogenesis and shed light on the diversity of their
29 associated molecular processes among species, including *Timema* stick insects.
30
31
32 INTRODUCTION
33
34 A key step in sexual reproduction is the generation of haploid cells. The transition from
35 diploidy to haploidy occurs in meiosis, a cellular process that ensures the maintenance of
36 ploidy levels between generations. During meiosis, chromosomes are inherited from a diploid
37 progenitor germ cell to produce four haploid gametic cells, through two rounds of cell division
38 (1). In males, these events are followed by the process of spermiogenesis, during which the
39 four meiotic products mature into sperm cells which then fuse with female gametes and
40 restore the diploid cellular state (2). While traditionally viewed as conserved across model
41 organisms, emerging studies reveal significant variation in meiotic and post-meiotic processes
42 underlying sperm maturation (2-6).
43
44 In a canonical depiction of meiosis, the early steps (i.e., prophase I) involve chromosome
45 condensation, pairing, synapsis, and recombination (1). These processes work together to
46 facilitate the segregation of chromosomes and formation of novel allele combinations (1).
47 However, the temporal and functional relationships between these steps can vary among

48 species. For example, some lineages exhibit achiasmatic meiosis, where homologous
49 chromosomes segregate without recombination, as is the case for *Drosophila* fruit fly males
50 (7). In organisms that do recombine, the temporal relationships between meiotic
51 recombination and synapsis can also vary, with dependence or independence of synapsis on
52 the occurrence of double-stranded breaks (DSBs) and recombination (8). Although
53 recombination plays a key role in homologous chromosome segregation, it appears that
54 different features can coexist. Yet, the evolutionary origins and causes of this variation remain
55 unclear (7, 9).
56
57 Another variable phenotype is observed during the early steps of meiosis and in species with
58 differentiated sex chromosomes such as in XY or X0 systems (i.e., without Y chromosome).
59 Here, sex chromosomes partially synapse or do not synapse at all (10). This phenomenon is
60 thought to trigger major transcriptional changes, by which sex chromosomes are
61 transcriptionally silenced during meiosis through a process known as meiotic sex
62 chromosome inactivation (MSCI) (11). However, there is extensive variation in these
63 transcriptional changes among species, with MSCI occurring in some species but not others
64 (12-16). Additionally, the timing and mechanisms of MSCI differ between species, preventing
65 the formulation of a general theory as to why MSCI occurred in the first place (11, 17) (see
66 the discussion section for a list of proposed hypotheses).
67
68 Following the recombination and sex chromosome inactivation processes, two rounds of cell
69 division ensure the proper segregation of each homologous chromosome and chromatid. This
70 process is mediated by centromeres—specific chromosomal regions where centromere
71 proteins bind to DNA and facilitate the attachment of the spindle microtubules (18). However,

72 the way centromeres are specified varies considerably among species (19). In most
73 eukaryotes, centromeres are confined to specific regions of the chromosomes and are
74 marked by the histone variant CenH3 (also known as CENP-A), which recruits other
75 centromere proteins before cell division (20). These organisms, known as monocentric
76 species, contrast with the holocentric species, where centromeres are specified along the
77 entire length of chromosomes (21). Furthermore, the loading of centromere proteins,
78 including CenH3, shows considerable diversity; they can be deposited through various
79 mechanisms, and in some species, they are even entirely absent (19, 22). How such changes
80 can evolve and how the cellular machinery adapts to ensure accurate chromosome
81 segregation remains poorly understood.
82
83 Finally, the process of sperm maturation (i.e., spermiogenesis) involves a series of
84 chromosomal regulation that include changes in transcription and DNA compaction. While
85 these events are essential for the transmission of genetic information across generations,
86 they also pose significant challenges for preserving genome integrity (23). Despite its
87 importance, it remains largely unclear whether sexual organisms address these challenges in
88 similar or different manners.
89
90 Understanding the diversity of meiotic and post-meiotic processes has become a critical
91 concern for identifying the elements essential for gamete production and elucidating the
92 proximate and ultimate mechanisms underlying the diversification of gametogenesis.
93 The stick insect genus *Timema* has emerged as a compelling system for exploring the diversity
94 of cellular processes linked to spermatogenesis (i.e., male meiotic and post-meiotic
95 processes), owing to two recently uncovered features during male meiosis (24, 25). First, the

96 centromere histone determinant CenH3 binds in a localized or chromosome-wide manner
97 depending on chromosomes and meiotic stages (25). Second, the X chromosome
98 demonstrated significant alterations in transcriptional activity over gonad development,
99 diminishing in overall gene expression as the meiotic program initiates (24). These findings
100 prompted us to investigate in more detail the cellular processes involved in *Timema* male
101 meiosis. While our main focus was on the species *Timema californium*, we also used a
102 comparative approach across different *Timema* species, covering over 30 MY of divergence
103 (26), and compared our findings with the cellular processes described in other organisms (see
104 Materials and Methods for the details and limitations in the species comparisons). This
105 approach allowed us to explore the diversity and spatiotemporal dynamics of different
106 cellular processes involved in recombination, meiotic sex chromosome inactivation and
107 chromosome segregation. Overall, our study unveils that despite a conservation in the
108 cytological processes governing spermatogenesis in *Timema*, the spatiotemporal dynamics of
109 the molecular machinery involved can vary considerably among species, particularly when
110 compared to model organisms.
111
112
113 RESULTS
114
115 ***Timema* chromosomes pair and initiate recombination before synapsis during male**
116 **prophase I**
117
118 Meiotic recombination is initiated by the formation of programmed DNA double-stranded
119 breaks (DSBs) that rapidly induce the phosphorylation of the histone variant H2AX (γH2AX)

120 and the recruitment of the recombinase Rad51 that is involved in homologous recombination
121 and mediates the single-strand invasion to repair DNA after DSBs (27, 28). To determine
122 whether DSB formation and homologous recombination are required for initiating synapsis
123 during *Timema* male meiosis, which is chiasmatic (29), we analysed the temporal localisation
124 of these two proteins, as well as the subunit of the cohesin complex SMC3. SMC3 marks
125 chromosomal axes but can also be used as marker for the progression of synapsis as SMC3
126 filaments become thicker as chromosomes pair and synapse (30). We find that the induction
127 of recombination, including DSB formation and DNA repair via strand invasion, starts prior to
128 synapsis, when chromosomes begin to condense and elongate into strands (see materials and
129 methods for the characterization of cellular stages). Indeed, during the early zygotene stage,
130 γH2AX and Rad51 form a cloud of foci at a polarized region of the nucleus (Figure 1A-E; Figure
131 2A-E; Supplementary figures 1A-J and 2A-O). At the same stage, only thin continuous SMC3
132 filaments are observed (Figure 1A-C; Figure 2A-C; Supplemental figure 3C), forming a
133 structure commonly referred to as the bouquet configuration in other species (31, 32). The
134 polarized patterns of γH2AX and Rad51 proteins as well as the bouquet configuration were
135 also observed in grasshopper spermatocytes (9), suggesting that the process is conserved
136 across the polyneopteran insect orders.
137 During the mid-zygotene to pachytene transition, synapsis progresses gradually and
138 asynchronously among chromosomes, alongside with the resolution of the induced DSBs. This
139 was evidenced by SMC3 filaments gradually shifting from thin to thicker filaments, with a
140 variable number of thick filaments among cells, while the γH2AX signal progressively
141 homogenizes and decreases over the entire nuclear surface (Figure 1F-O; Supplemental figure
142 1A-O; Supplemental figure 3E-J). Similarly, the Rad51 signal decreases and only a subset of

143 recombination sites per chromosome persists as discrete foci along the thick SMC3 filaments
144 (Figure 2F-T; Supplemental figure 2A-E and 2P-T).
145 Before the initiation of the first meiotic division, γH2AX and Rad51 signals disappear while
146 SMC3 filaments become interrupted near chromosomal ends (Figure 1P-T; Figure 2Z-Zd;
147 Supplementary figure 3O-P and 3A'-O'). These interruptions likely highlight chiasma sites that
148 correspond to the contact zone where homologous chromosomes remain connected (33). At
149 metaphase I, chromosomes then form "rod" bivalents with cross-shaped SMC3 labeling
150 interrupted at one chromosomal end for the majority of chromosomes in all four *Timema*
151 species examined, suggesting the formation of a single terminal or sub-terminal chiasma site
152 (Supplementary figure 3O-P and 3A'-L'). We also identified two *Timema* species forming one
153 "ring" bivalent with more circularized SMC3 labeling interrupted at two chromosomal ends,
154 suggestive of two terminal or sub-terminal chiasma sites (Supplementary figure 3O-P and 3A'-
155 F').
156
157 Overall, our findings show that the phosphorylation of the histone H2AX and the
158 chromosomal deposition of the recombinase Rad51 occur prior to the thickening of SMC3
159 filaments, supporting the idea of a recombination-dependent machinery for synapsis
160 formation as observed in *Arabidopsis,* yeast, jellyfish and mouse (34-37). Furthermore, the
161 terminal positions of chiasma sites suggest that crossing-overs may preferentially occur on
162 chromosomal ends in *Timema* males, although such conclusion requires further molecular
163 evidence.
164
165
166 **Spermatogenesis progression of meiotic sex chromosome inactivation in *Timema* males**

167

168 In *Timema* male meiosis, the X chromosome remains unsynapsed due to the absence of a
169 homologous partner (i.e., X0 system) (38). As a result, the pachytene stage is marked by thick
170 SMC3 filaments on all chromosomes except the X chromosome, where a thin SMC3 filament
171 remains (Supplementary figure 3I) (see materials and methods for X vs autosome
172 identification). At the same stage, we observed that the X chromosome is also characterized
173 by an intense DAPI staining, not present at the zygotene stage (Supplementary figure 3C-J).
174 This is reminiscent of the heteropycnotic body (also termed sex body) found in organisms
175 with meiotic sex chromosome inactivation (MSCI) (16, 39). The heteropycnotic body is a key
176 marker of MSCI, highlighting the intense compaction of sex chromosomes, and is often
177 assisted by the DNA damage response (DDR) pathway in mammals, where diverse DDR factors
178 including γH2AX and Rad-related kinases accumulate to initiate the chromosome-wide
179 silencing (15, 40). However, this pathway appears to be modified in hemipteran and
180 orthopteran insects, notably with the absence of Rad51 and the emergence of γH2AX only
181 after the sex body has formed (16, 41, 42). Our analyses of γH2AX and Rad51 in *Timema*
182 suggest that this cascade is also modified compared to both insects and mammals. Indeed,
183 despite the detection of Rad51 proteins as discrete sites along the unsynapsed axial element
184 of the X chromosome (Figure 2P-T; Supplementary figure 2A-E and 2P-T), the γH2AX signal is
185 inconsistently detected across *Timema* species during pachytene (Figure 1K-O;
186 Supplementary figure 1A-O). Specifically, *T. californicum* and *T. petita* exhibit two to three
187 distinct γH2AX patches in X regions, while no signal is detected on the X chromosome for *T.*
188 *cristinae* and *T. chumash*. Note that because we used a commercial antibody against γH2AX,
189 we cannot formally exclude that this variation across species is caused by variable antibody
190 affinities. However, the antibody clearly detects the expected cloud of DSB-associated γH2AX

191 foci at a polarized region of the nucleus during the zygotene stage in all species (Figure 1A-E;
192 Supplementary figure 1A-J). We could also verify that the presence or absence of γH2AX on
193 the X chromosome at pachytene is consistent across individuals of the same species
194 (Supplementary table 1). Finally, the X chromosome in all *Timema* species exhibits intense
195 DAPI staining at the nuclear periphery, attesting that the unusual γH2AX pattern on the X
196 chromosome, in some species, does not prevent the tight compaction of this chromosome
197 (Figure 1N-O; Supplementary figure 1A-O).
198 We previously showed that the X chromosome compaction in pachytene is associated with
199 MSCI (24). However, it is unknown whether the X chromosome in *Timema* is transcriptionally
200 inactive throughout spermatogenesis or only at specific stages, including the pachytene stage.
201 To determine the transcriptional status of the X chromosome and autosomes, we immuno-
202 labelled the RNA polymerase II phosphorylated on serine 2, which is a conserved
203 transcriptional marker of transcription elongation (43). We found that the X chromosome
204 remains transcriptionally inactive throughout spermatogenesis, while there are two phases
205 of autosomal transcription during meiosis and spermiogenesis. Indeed, the RNA polymerase
206 II signal is first absent from the entire nucleus at the onset of prophase I (i.e., leptotene and
207 zygotene stages; Figure 3A-J). It then appears at the pachytene stage only on the autosomes,
208 concomitantly with the formation of the heteropycnotic body (Figure 3K-O). This first
209 transcriptional phase is maintained until the diplotene stage (Figure 3P-Zi) and is followed by
210 a second transcriptional phase during the spermatid stage, marked again by an intense RNA
211 polymerase II signal on the autosomes but not the X chromosome (Figure 3a-e'). As
212 spermatids then elongate, the polymerase II signal is depleted from the nuclei and the
213 heteropycnotic body is no longer visible (Figure 3f-o).

214 Contrasting with the absence of polymerase II signal, we observed that the X chromosome
215 becomes coated by the modified histone H3K9me3 in pachytene (Figure 4F-J; Supplementary
216 figure 4A-F and 4O-S), another MSCI marker involved in transcriptional repression,
217 heterochromatization, and heteropycnotic body formation of the sex chromosomes during
218 MSCI (16, 40). However, while the heteropycnotic body persists in all species until the round
219 spermatid stage, the maintenance of H3K9me3 on the X varies among species: it remains until
220 the round spermatid stage in *T. petita* and *T. chumash* whereas its signal is already lost at this
221 stage in *T. californicum* and *T. cristinae* (Figure 4 a-e'; Supplementary figure 4A-C and 4G-S).
222 We note that species lacking H3K9me3 signal on the X chromosome at the spermatid stage,
223 display a coating of H3K9me3 on the X chromosome in pachytene and other meiotic stages
224 such as metaphase I (Figure 4F-T; Supplementary figure 4A-C), indicating that the binding
225 efficiency of the antibody is not affected in these species.
226
227 Combined, our findings show the complete transcriptional inactivity of the X chromosome
228 throughout *Timema* spermatogenesis, which explains the strongly reduced overall gene
229 expression of the X chromosome compared to autosomes in male gonads (24). Furthermore,
230 the establishment and maintenance of this process appear to be dynamic, unfolding across
231 five major cellular steps. During the first step, the polymerase II is absent from nuclei in
232 leptotene and zygotene stages, and all chromosomes, including the X chromosome, are most
233 likely transcriptionally inactive (Figures 3A-J). The second step involves the appearance of the
234 MSCI markers such as the formation of the heteropycnotic body along with the presence of
235 H3K9me3, γH2AX and Rad51 proteins on the X (Figure 1K-O; Supplementary figure 1A-O;
236 Figure 2P-T; Supplementary figure 2A-T). While this process appears to depend on H3K9me3
237 and Rad51 (as in mammals (15)), it does not seem to require the accumulation of γH2AX on

238 the X chromosome (resembling the pattern in grasshoppers but differing from that in
239 mammals (15, 41)). However, further functional validations such as knockdown or knockout
240 experiments will be required in the future, as currently not accessible in the system, to draw
241 firm conclusions on the mechanisms associated with the initiation of MSCI in *Timema*. The
242 second step is also marked by a first wave of transcription on the autosomes from pachytene
243 to diplotene, while the X chromosome is maintained transcriptionally silenced throughout
244 this entire period (Figure 3K-T). In the third step, transcription is once again greatly reduced
245 or entirely absent across all chromosomes during metaphase I. However, unlike in the first
246 step, the X chromosome can be distinguished from the others due to the presence of
247 H3K9me3 modification coating its entire length (Figure 3U-Y; Figure 4P-T; Supplementary
248 figure 4D-F). This enrichment of H3K9me3 modification on the X chromosome, compared to
249 the autosomes, was previously shown and quantified for *Timema* male meiosis using
250 H3K9me3-directed ChIP-seq analyses (24). The fourth step marks the presence of the
251 heteropycnotic body until the round spermatid stage and the initiation of the second wave of
252 autosomal transcription (Figure 3a-e'). This step is also marked by some variation in the
253 maintenance of H3K9me3 among *Timema* species (Figure 4a-e'; Supplementary figure 4A-C
254 and 4G-S), suggesting that this epigenetic modification is not essential for the maintenance
255 of X silencing at this stage. Moreover, we note that H3K9me3 signals in the autosomes vary
256 among species at this and earlier stages, with for instance the presence of intense foci in the
257 nuclei of *T. petita* or *T. cristinae* that might indicate clusters of heterochromatin regions
258 (Supplementary figure 4A-C and 4O-S). Finally, the last step involves the loss of MSCI and
259 transcriptional markers in all species as spermatids elongate and maturate, as evidenced by
260 the absence of the heteropycnotic body, as well as the loss of RNA polymerase II and
261 H3K9me3 signals (Figure 3f-o; Figure 4f-o; Supplementary figure 4D-F).

262

263

264 **Dynamics and assembly of centromere proteins during spermatogenesis**

265

266 Interestingly, the first wave of transcription in *Timema* does not only coincide with the
267 initiation of MSCI but also with a change in chromosomal distribution of the centromere
268 histone variant CenH3, which we described previously (25). Specifically, *Timema* is a
269 monocentric species and its CenH3 is expected to localize to confined chromosomal regions,
270 where it recruits other centromere proteins to ensure proper chromosome segregation
271 during cell division (18, 25). However, we find that the absence of transcription from
272 autosomes and the X chromosome during leptotene and zygotene in meiosis I coincides with
273 the recruitment of CenH3 along the full length of all chromosomes (Figure 3A-J; Figure 5A-J
274 but also (25)). It is only during the transition from zygotene to pachytene that cells establish
275 the expected monocentric distribution of CenH3 on the autosomes but not on the X, which
276 we here show occurs in parallel to the activation of transcription from the autosomes and
277 silencing of the X (Figure 3K-O; Figure 5K-O; Supplementary figure 5).
278 Considering this parallel occurrence, we examined whether a broader correlation could exist
279 between transcription and the recruitment of centromere proteins in *Timema*. For this, we
280 extended our previous observations on CenH3 to include other centromere proteins and
281 additional stages of spermatogenesis (i.e., not examined in (25)). This allowed us to integrate
282 the recruitment dynamics of CenH3 and other centromere proteins with the progression of
283 spermatogenesis, which has generally been poorly assessed.

284

285 We first analyzed the recruitment dynamics of CenH3 on autosomes and the X chromosome
286 during prophase I and evaluated its conservation across *Timema* species, as our previous
287 observations focused on a single species at this stage (25). We found that once meiosis
288 initiates (i.e., lepto- to zygotene stage), CenH3 is recruited over the entire length of every
289 chromosome in all *Timema* species (Figure 5A-J; see Supplementary figure 6 for CenH3 signal
290 before meiosis; Supplementary figure 7A-I), confirming that the longitudinal recruitment is
291 evolutionarily conserved in this clade. However, the shift of CenH3 from a longitudinal
292 distribution to a single focus on the X occurs only after the first meiotic division, not during
293 prophase I as seen in autosomes (a detailed characterization of CenH3 dynamics on the
294 autosomes during prophase I was previously documented in (25), but can still be visualized in
295 Figure 5A-T; see Figure 5U-Zd for the shift of CenH3 on the X). Moreover, this shift is not
296 accompanied by an activation of transcription as the X remains silenced beyond the first
297 meiotic division (Figure 3U-Zd; Figure 5U-Zd). Thus, although the distribution of CenH3 and
298 transcriptional activity are correlated on the autosomes, this is not the case for the X, where
299 the loss of the longitudinal distribution of CenH3 from anaphase I onwards is not
300 accompanied by a transcriptional activation (Supplementary figure 5).
301
302 We then investigated whether the anti-correlation observed between transcription and
303 CenH3 recruitment on autosomes during early meiosis also applies to other centromere
304 proteins. We characterized the chromosomal distribution of two kinetochore proteins, one
305 from the inner (CenpC) and one from the outer region (Ndc80), as well as the Bub1 protein
306 from the spindle assembly checkpoint (SAC) (44-46). However, none of the three proteins are
307 present at early prophase stages (i.e., lepto- and zygotene stages) (Figure 6A-J; Figure 7A-O;
308 Figure 8A-J), indicating that lack of transcription does not support the recruitment of these

309 proteins at these stages. Instead, we observed that CenpC binds in a monocentric fashion on
310 all chromosomes from pachytene until the end of the first meiotic division (Figure 6K-Y;
311 Supplemental figure 8A-O), revealing that the recruitment of this inner kinetochore protein,
312 which directly interacts with CenH3 in other organisms (19), cannot be solely attributed to
313 CenH3 deposition during male meiosis in *Timema*. On the other hand, the outer kinetochore
314 protein Ndc80 and SAC protein Bub1 load in a monocentric fashion on every chromosome
315 only at pro-metaphase I, which corresponds to the stage of nuclear-envelope breakdown in
316 several organisms (Figure 7P-T; Figure 8K-T; Supplemental figure 9P-T; Supplemental figure
317 10A-E). The meiotic regulation of these two proteins and associated complexes have only
318 been studied in a handset of species (44, 47), yet our findings are consistent with the idea
319 that the assembly of the outer kinetochore region is tightly regulated in time, taking place
320 just before segregation to prevent premature microtubule–kinetochore interactions (48).
321 During the second meiotic division, all four centromeric proteins are found to localize to
322 centromeres (Figure 5Ze-Zi; Figure 6Z-Zi; Supplementary figure 8A-E; Supplementary figure
323 9F-J; Supplementary figure 10F-J). However, their timing of unloading differs. CenpC and Bub1
324 unload rapidly after the second meiotic division, as evidenced by the loss of signal from the
325 round spermatids onwards (Figure 6a-o; Figure 8a-o; Supplementary figure 8A-E). By
326 contrasts, the CenH3 signal is maintained until the elongated spermatid stage but absent from
327 all chromosomes in mature sperm cells (Figure 5a-o; Supplementary figure 7A-I), which is
328 either caused by an active removal of the protein as in *Drosophila virilis* and *Caenorhabditis*
329 *elegans* (49, 50), or because the chromatin is too compacted at this stage for antibody
330 accessibility. Finally, Ndc80 displays a surprising cellular pattern after meiosis, accumulating
331 in a few regions until the formation of mature sperm cells where it disappears (Figure 7a-o).
332 Although this cellular localization remains unexplained, it is very unlikely to reflect clustering

333 of centromeres as they appear distinctly visible when marked with the CenH3 protein at this
334 stage (Figure 5a-j).
335
336 Taken together, this study represents one of the rare instances describing the cellular
337 dynamics of essential centromere proteins during spermatogenesis, revealing that the
338 regulation of chromosomal loading and unloading of these proteins is tightly regulated in
339 space and time. Initially, CenH3 distributes along the entire length of all chromosomes while
340 the other centromere proteins are absent (Figure 5A-J; Figure 6A-J; Figure 7A-J; Figure 8A-J).
341 This is then followed by focal restriction of CenH3 on each autosome and monocentric
342 recruitment of CenpC on all chromosomes (autosomes and the X chromosome) during
343 synapsis (Figure 5K-O and Figure 6K-O). Just before the first cellular division, the last
344 components of the kinetochore and SAC proteins are recruited in a monocentric fashion,
345 forming the active centromeres that attach to spindle microtubules during metaphase I
346 (Figure 7P-T; Figure 8K-T; Supplementary figure 9A-E and K-T; Supplementary figure 10A-E;
347 see also (25)). Finally, by the end of the second meiotic division, kinetochore and SAC
348 complexes disassemble, leaving only the CenH3 proteins within the centromere regions
349 (Figure 5a-j; Figure 6a-j; Figure 7a-j; Figure 8a-j).
350 In addition to linking centromere protein loading with the progression of spermatogenesis,
351 our study builds upon previous research on univalent chromosome segregation in praying
352 mantis and grasshoppers, where kinetochore and SAC proteins are differently regulated (51-
353 53). In *Timema*, no differences in kinetochore or SAC proteins were identified between the X
354 chromosome and autosomes, although expanding this comparison to other centromere
355 proteins will be necessary in the future to draw conclusions on their actual involvement.
356

357

358 DISCUSSION

359

360 The regulation of chromosome dynamics during spermatogenesis is essential for male
361 reproductive success. Yet, the cellular processes underlying this regulation and how they
362 evolve across species remains poorly understood. Our data offer new insights in this regard,
363 by first revealing that chromosome synapsis in *Timema* follows recombination. This pattern
364 may represent the ancestral state in eukaryotes as it is present in yeast, *Arabidopsis,* jellyfish
365 and mouse (34-37) but absent in only *D. melanogaster* and *C. elegans* (54, 55). It may also
366 reflect the ancestral state in insects. Indeed, only in female meiosis of *Drosophila* (Diptera
367 order) is synapsis known to precede recombination (7, 8). In species of three additional insect
368 orders, male meiotic progressions mirror our descriptions in *Timema* (Orthoptera:
369 *Eyprepocnemis plorans* (9, 16); Hemiptera: *Graphosoma italicum* (56); Lepidoptera: *Bombyx*
370 *mori* (57)). Nevertheless, the discrepancy in timing of recombination between *Drosophila* and
371 other insect lineages may also originate from differences in meiotic prophase I between males
372 and females (58, 59). Thus, further studies on female meiosis in additional insect orders will
373 be required before drawing firm conclusions on the evolution of recombination and synapsis
374 in insects.

375

376 We also reveal that the lack of synapsis in *Timema* male meiosis is associated with the
377 initiation of MSCI on the X chromosome, as shown in several organisms, including mammal
378 and insect species (11, 16). However, the persistence of a complete transcriptional inactivity
379 of the X chromosome throughout *Timema* spermatogenesis questions the driving forces
380 behind the origin of the MSCI process. The evolution and key function of MSCI continues to

381 be a source of theories and speculations, with different proximate and ultimate hypotheses
382 proposed.
383 A first hypothesis posits that MSCI primarily operates to shelter unsynapsed region(s) on the
384 sex chromosomes during the first meiotic division. Indeed, different factors generate a need
385 for such sheltering, including damaging effects of unrepaired DSBs or ectopic recombination
386 as well as circumventing cellular checkpoints that are active during prophase I (40, 60, 61).
387 Our findings allow us to exclude at least two such factors. First, MSCI does not appear
388 necessary to shelter the X from the induction of DSBs during meiosis in *Timema*. Indeed, MSCI
389 begins at a later stage than the initiation of DSBs (illustrated by the phosphorylation of H2AX
390 in leptotene), meaning that MSCI cannot protect the X from the induction of DSBs. This
391 contrasts with findings in other species such as the grasshopper *Eyprepocnemis plorans* where
392 MSCI precedes the γH2AX signal on the X (16). Secondly, MSCI does not solely serve to
393 circumvent checkpoints during meiosis. This is revealed by the fact that the *Timema* X
394 chromosome maintains its condensation state and transcriptional inactivation long after the
395 first meiotic division (i.e., until spermiogenesis and significantly past putative checkpoints),
396 suggesting that other factors are involved in maintaining the X transcriptionally silenced.
397 A second, mutually non-exclusive hypothesis postulates that MSCI functions to
398 transcriptionally silence some or all genes on the sex chromosomes that could impact cell
399 survival during various stages of spermatogenesis and post-spermatogenesis (11, 60). Our
400 investigation of MSCI in *Timema* supports this hypothesis, revealing that the X chromosome
401 remains silent throughout meiosis and MSCI markers emerge only when meiotic transcription
402 activates in pachytene. Similarly, we identified in the literature that MSCI markers are
403 typically found in species where transcription activates during meiosis (this is notably the case
404 in mice, opossum or grasshoppers) (14-16), while MSCI markers appear to be absent in

405 species such as platypus or chicken, where global transcription is low during meiosis (12, 13).
406 In *Timema*, we further show that a transcriptional activity post-meiosis would be sufficient to
407 explain the maintenance of the X-silencing status until the round spermatid stage. Indeed,
408 during this cell stage, a transcription of X-linked genes would be expected to result in major
409 expression differences between nullo-X and X-containing spermatids. Our interpretations are
410 again supported by findings in mice, opossum or grasshoppers, which are also characterized
411 by transcriptional repression of sex chromosomes post-meiosis (also termed postmeiotic sex
412 chromatin (PMSC)) (11, 14, 16, 62).
413 Overall, the cell biology of MSCI in *Timema* indicates that a hypothesis based on the sheltering
414 of unsynapsed chromosomes during meiosis I is not sufficient to fully explain MSCI and that
415 active repression of X-linked genes throughout spermatogenesis likely plays an important
416 role.
417
418 Finally, we show that the *Timema* X chromosome differs not only from autosomes by its
419 transcriptional activity but also chromatin organization. Indeed, the histone variant CenH3
420 binds to the X along its entire length from pachytene to metaphase I, while autosomes have
421 CenH3 only located at their centromeres during these meiotic stages (Figure 5K-Y and
422 Supplementary figure 7 but also (25)). These distinct distribution patterns raise important
423 questions about the mechanisms regulating the deposition and removal of CenH3, which are
424 known to be complex and variable among species (63).
425 Taken together, our findings allow us to examine three proposed mechanisms for CenH3
426 deposition, which involve kinetochore proteins, transcriptional activity, or SMC proteins (50,
427 63, 64). While the first two mechanisms appear to be either incompatible or only partially
428 applicable to *Timema*, the third mechanism aligns well with our observations. Specifically, the

429 kinetochore-mediated recruitment of CenH3 has been identified in monocentric lineages,
430 where specific centromere proteins—such as the kinetochore protein CenpC—play a key role
431 in recruiting CenH3 during both mitosis and meiosis, as observed in chicken, humans, and
432 *Drosophila* (19, 65). However, our findings exclude this hypothesis in *Timema*: we observe
433 CenH3 recruitment first, followed by the subsequent appearance of three other centromere
434 proteins (i.e., CenpC, Ndc80, and Bub1), whereas this order should be reversed under a
435 kinetochore-driven model. The transcription-based mechanism has been described in *C.*
436 *elegans*, where CenH3 deposition occurs in regions with low or no transcriptional activity (50).
437 This low transcriptional activity (or lack thereof) may account for CenH3 deposition along all
438 chromosomes in leptotene and its removal from autosomes in pachytene. However, it fails to
439 explain the removal of Cenh3 along the X in anaphase I (Figure 3A-Zd; Figure 5A-Zd;
440 Supplementary figure 5). Instead, our data strongly support a third mechanism based on SMC
441 proteins, as proposed in a recent model, where these proteins block and anchor interactions
442 with centromeric nucleosomes during loop extrusion and yield a holocentric-like
443 chromosome via chromatin condensation (64). The observed dynamics of CenH3 in *Timema*
444 male gonadal cells closely match these model predictions. While CenH3 filaments form when
445 SMC3 proteins appear and run along the length of every chromosome during leptotene, the
446 CenH3 filament on the X chromosome disappears when SMC3 retires from chromosomal axes
447 in anaphase I. Interestingly, similar dynamics may also support this mechanism in certain
448 holocentric lineages, where centromere proteins first localize between homologs, in
449 association with axis proteins such as the cohesin complex, before relocating to more
450 poleward-facing positions (66-68).
451

452 Overall, this study highlights the importance of exploring beyond traditional model systems
453 in cell biology to better understand the diverse processes governing male gamete formation
454 and chromosomal inheritance. Moreover, it offers essential insights to reconstruct the
455 evolutionary steps that have shaped this diversity.
456
457
458 MATERIAL AND METHODS
459
460 Timema Sample Collection
461
462 We used wild-collected individuals of the species *T. douglasi* (38°57'24.9"N 123°32'10.0"W),
463 *T. knulli* (35°50'10.3"N 121°23'29.3"W), *T. petita* (36°21'32.0"N 121°54'01.3"W), *T. californicum*
464 (37°20'35.4"N 121°38'11.3"W), *T. cristinae* (34°32'25.4"N 119°14'20.5"W), *T. monikensis*
465 (34°06'53.6"N 118°51'11.3"W), *T. bartmani* (34°09'48.1"N 116°51'43.5"W) and *T. chumash*
466 (34°06'53.6"N 118°51'11.3"W).
467
468 Design, selection and validation of antibodies
469
470 A combination of custom and commercially available antibodies was employed for the
471 immunostaining assays (Supplementary table 2). A polyclonal rabbit anti-SMC3 antibody
472 (Chemicon International) raised against a synthetic peptide from human SMC3 was used to
473 detect SMC3. To detect γ-H2AX we used a monoclonal mouse antibody (Upstate) raised
474 against amino acids 134–142 of human histone γ-H2AX (69). This sequence has 8 identical
475 amino acids in yeast and mouse (70). A polyclonal rabbit anti-Rad51 antibody (Ab-1; PC130;

476 Oncogene Research Products), generated against recombinant HsRad51 protein, was used to
477 detect Rad51. All three antibodies exhibited expected and similar cytological patterns to
478 those observed in grasshoppers (9, 41, 71), with notably the presence of SMC3 in filaments
479 as well as γ-H2AX and Rad51 in foci at the nuclear portion where chromosome ends clustered
480 during prophase I (i.e., bouquet stage).
481 The presence of X heterochromatization and transcriptional activity in *Timema* male gonads
482 has previously been tested in (24), and similarly determined in the present study, using
483 antibodies against either H3K9me3 (#AB8898, AbCam; which labels silencing
484 heterochromatin marks) or RNA polymerase II phosphorylated at serine 2 (p-RNApol-II
485 (ab193468, AbCam); an indicator of transcription).
486 Details of the custom antibody designs for *Timema* CenH3 and kinetochore proteins can be
487 found in (25) and in the Supplementary table 2. For the SAC protein Bub1, we first used the
488 protein sequence of *Drosophila melanogaster* to identify orthologs in stick insects via Protein
489 BLAST against the NCBI database. A blast hit was already annotated as Bub1 in the stick insect
490 *Bacillus rossius redtenbacheri* (XP_063234342.1) and was further used to identify orthologs
491 in *Timema* via Protein BLAST against the NCBI database. The best hits of nine *Timema* species
492 corresponded to the Bub1 ortholog as revealed by Protein BLAST against the non-redundant
493 NCBI database. We then used the protein sequence from *T. poppense* (CAD7396045.1) to
494 outsource to Covalab (Lyon, France) the design of three distinct peptide sequences
495 (Supplementary table 2). For all custom antibodies, Covalab developed polyclonal rabbit
496 antibodies from the designed peptides, purified them via a sepharose column, and tested
497 their specificity and immunoreactivity using ELISA assays. Moreover, all custom antibodies
498 displayed confined signals in *Timema* male chromosomes at metaphase I, where spindle
499 microtubules attach, consistent with the expectations for monocentric species (72).

500

501 Immunostaining procedure with SMC3 antibody

502

503 Male gonads display a morphology resembling grapes, comprising a shoot housing mature
504 sperm cells and an oval structure encapsulating cells at various meiotic stages (see (25)).
505 Gonads from alive adults were dissected in 1X PBS, fixed in a solution containing 2%
506 paraformaldehyde and 0.1% Triton X-100 for 15 minutes, followed by gentle squashing of 4-
507 5 "grapes" onto poly-L-lysine-coated slides, then rapidly immersed in liquid nitrogen
508 (according to (73)). After a 20-minute incubation in 1X PBS, tissues on slides were subjected
509 to blocking with 3% BSA (in 1X PBS (w/v)) blocking buffer for a minimum of 30 minutes.

510

511 Immunostaining started by incubating slides with diluted primary antibodies in 3% BSA
512 overnight at 4°C within a humid chamber. Exception was made for the already fluorescently
513 labeled SMC3 antibody that was added after the following blocking step (see below). Detailed
514 information for all antibodies used, including working concentrations, are provided in
515 Supplementary table 2. Subsequently, slides underwent three 5-minutes washes in 1X PBS,
516 followed by a 1-hour incubation with the secondary antibody, diluted at a ratio of 1:150 in 3%
517 BSA, at room temperature. Slides were then washed thrice for 5 minutes each, followed by a
518 10-minute wash in 1X PBS.
519 As most primary antibodies were developed from the same host (i.e., rabbit), a blocking step
520 was performed using diluted Normal Rabbit Serum (NRS 5%) for 30 minutes at room
521 temperature, followed by a 10-minute wash in 1X PBS. Subsequently, slides underwent a 1-
522 hour incubation at room temperature with the already fluorescently labeled SMC3 antibody

523 diluted at 1:100. Slides were washed thrice in 1X PBS, stained with DAPI for 3 minutes, washed
524 one last time 5 minutes in 1X PBS, and mounted in Vectashield media.
525
526 Immunostaining procedure without SMC3 antibody
527
528 For this procedure, no blocking steps were performed (i.e. without 3% BSA and NRS).
529 Therefore, after a 20-minute incubation in PBS, tissues on slides were directly incubated with
530 diluted primary antibodies in 1X PBS overnight at 4°C within a humid chamber. Exception was
531 made for the already fluorescently labeled **α**-tubulin antibody that was used in the following
532 step (with the secondary antibody). Slides were then washed thrice for 5 minutes each in 1X
533 PBS, followed by a 1-hour incubation with the secondary antibody or the already fluorescently
534 labeled **α**-tubulin antibody (when needed), diluted at a ratio of 1:150 in 1X PBS, at room
535 temperature. Slides were washed thrice in 1X PBS, stained with DAPI for 3 minutes, washed
536 one last time 5 minutes in 1X PBS, and mounted in Vectashield media.
537
538 Image acquisition
539
540 All acquisitions were performed using the Zeiss LSM 880 airyscan confocal microscope
541 equipped with a 60x/oil immersion objective. All acquisitions were produced by the
542 superimposition of focal planes. Post-processing, including cropping and pseudocoloring, was
543 carried out using Fiji (74).
544
545 Characterization of spermatogenetic stages and X chromosome identification
546

547 All prophase I stages could be determined based on the cellular patterns observed for SMC3.
548 Specifically, the entry of meiosis is characterized by numerous and thin SMC3 filaments that
549 mark the chromosomal axes of each chromosome before homologs have paired
550 (Supplementary figure 3A; (71)). The bouquet stage is evidenced by the cluster of
551 chromosome ends forming SMC3 loops, as well as the appearance of DNA strands with DAPI
552 staining (Supplementary figure 3C-D). The progression of synapsis during zygotene is
553 evidenced by the combination of thin and thick SMC3 filaments within the same nucleus
554 (Supplementary figure 3E-H). The pachytene stage is marked by thick SMC3 filaments, except
555 on the X chromosome where SMC3 remains thin and the DAPI staining becomes intense (see
556 below for details on X chromosome identification; Supplementary figure 3I-J). Metaphase I
557 and anaphase I differ by the distribution of SMC3 proteins, which stain either along
558 chromosome axes or near centromeres, respectively (Supplementary figure 3O-R). Moreover,
559 metaphase I is characterized by a monopolar orientation of the X chromosome that does not
560 align on the metaphase plate, contrary to autosomes (Supplementary figure 3O-P).
561 Prophase II is characterized by round nuclei with SMC3 foci that stain again near centromeres
562 (Figure 5Ze-Zi). Metaphase II keeps the SMC3 foci but has no longer the X chromosome
563 segregating as unipolar as in meta-/anaphase I (Supplementary figure 3S-T), while cells in
564 anaphase II loss the SMC3 foci and the number of DAPI-stained chromosomes is reduced
565 (Supplementary figure 3U-V).
566 Spermatids have several distinct features that involve the absence of SMC3 staining
567 (Supplementary figure 3a-f), a developing flagellum visible with α-tubulin staining
568 (Supplementary figure 3A''-C''), and a smaller nucleus size for the round spermatids as
569 compared to meiotic cells (Supplementary figure 3b and 3b').
570

571 The cytological identification of the X chromosome was previously characterized by joint
572 analyses between cytological observations of CenH3 and H3K9me3, as well as ChIP-seq data
573 on these same proteins (24, 25). This allowed us to further characterize the X chromosome as
574 the chromosome with intense DAPI staining in the nucleus.
575
576 Limitations of the study
577
578 *Timema* are non-model organisms with a one-year generation time, reaching sexual maturity
579 at different times during the spring depending on geographical location, and with adult
580 tissues only available for a brief period. Additionally, *Timema* are difficult to rear under
581 laboratory conditions, and each individual produces a limited number of meiotic cells at
582 various stages, with the majority being in the pachytene stage. These constraints limit the
583 ability to perform consistent staining across all species and stages. However, the evolutionary
584 dynamics of various cellular processes, within this insect group, can still be inferred by
585 sampling a subset of *Timema* species representing the different clades ((75); Supplementary
586 table 3). When inter-species variation is observed (e.g., for γH2AX and H3K9me3 signals on
587 the X chromosome; see Supplementary table 1 and 3), its reliability was assessed by sampling
588 multiple individuals from the same species and confirming consistent phenotypes in at least
589 two different species.
590
591
592 ACKNOWLEDGEMENT
593 We thank current and previous members of the Schwander lab for discussions. We also thank
594 Rocío Gómez Ortega for help in developing the immunostaining protocol in *Timema*, and

Arnaud Paradis from Cell Imaging Facility (CIF, Lausanne University, Switzerland) for help with image acquisitions. **Funding**: We would like to acknowledge funding from the European Research Council Consolidator Grant (No Sex No Conflict to T.S.) and Swiss FNS grant 31003A_182495 (T.S.). **Author contributions**: Z.D., W.T. and T.S. designed the study. Z.D. and W.T. performed molecular work. Z.D. developed methods with input from M.D.. Z.D. and W.T. analyzed the data with input from T.S. and M.D.. W.T. and T.S. wrote the paper with input from all authors.

FIGURES

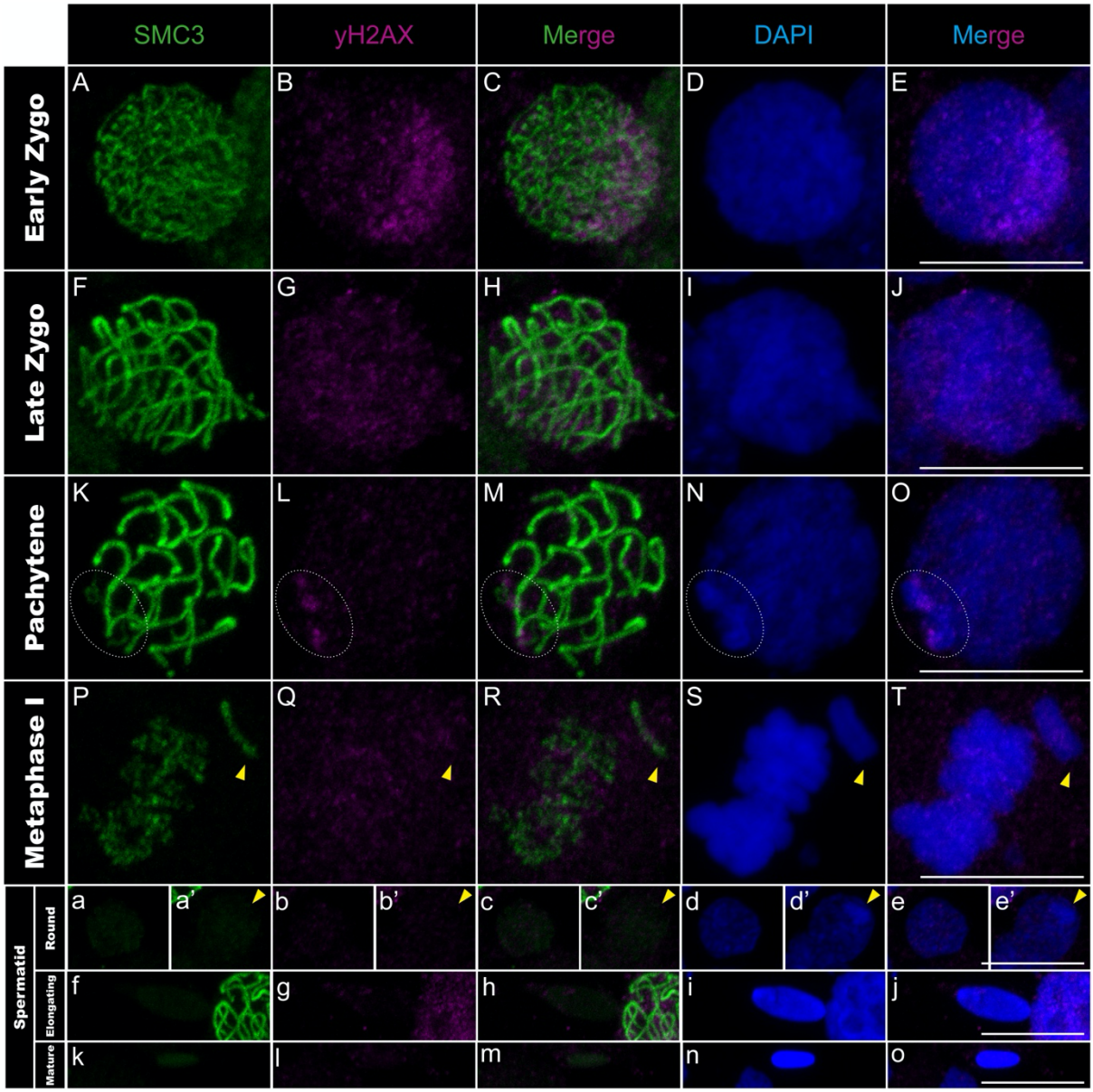

Figure 1: γH2AX distribution in *T. californicum* meiocytes and spermatids. Projections of stack images acquired across *T. californicum* squashed meiocytes (A–T) and spermatids (a–o), at the stages indicated, stained with DAPI (blue) and double immunolabeled for SMC3 (green) and γH2AX (magenta). γH2AX labeling is intense and granular in one nuclear pole, then gradually homogenizes and decreases as synapsis progresses, except on the X chromosome where three patches form in pachytene. The position of the X chromosome is indicated with arrowheads or dashed circles in pachytene (see materials and methods for X vs autosome identification). Scale bar: 10 µm. See Supplementary figure 1 for screens in males of other *Timema* species.

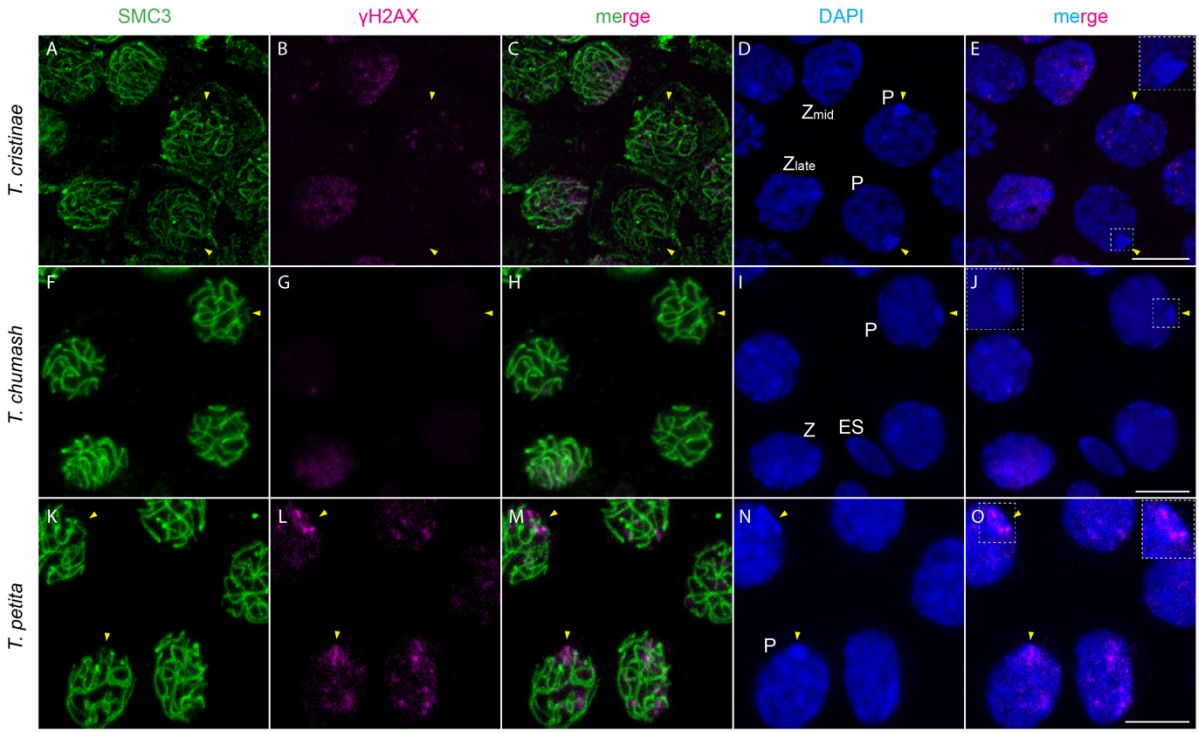

616

617 **Supplementary figure 1:** γH2AX distribution at various stages of spermatogenesis for three additional
618 *Timema* species, acquired through the projection of stack images. Focal cells at the zygotene stage are
619 labeled with the letter *Z*, cells at the pachytene stage with the letter *P*, elongated spermatid cells with
620 the letters ES, while yellow arrows indicate the X chromosome. Note that at the zygotene stage, the
621 γH2AX signal is observed at a polarized region of the nucleus, whereas at the pachytene stage, the X
622 chromosome in *T. petita* displays γH2AX patches as in *T. californicum*, but no signal was detected in *T.*
623 *cristinae* and *T. chumash*. A close-up view of the X chromosome is also shown within dashed squares
624 for each species. Scale bar: 10 µm.

625

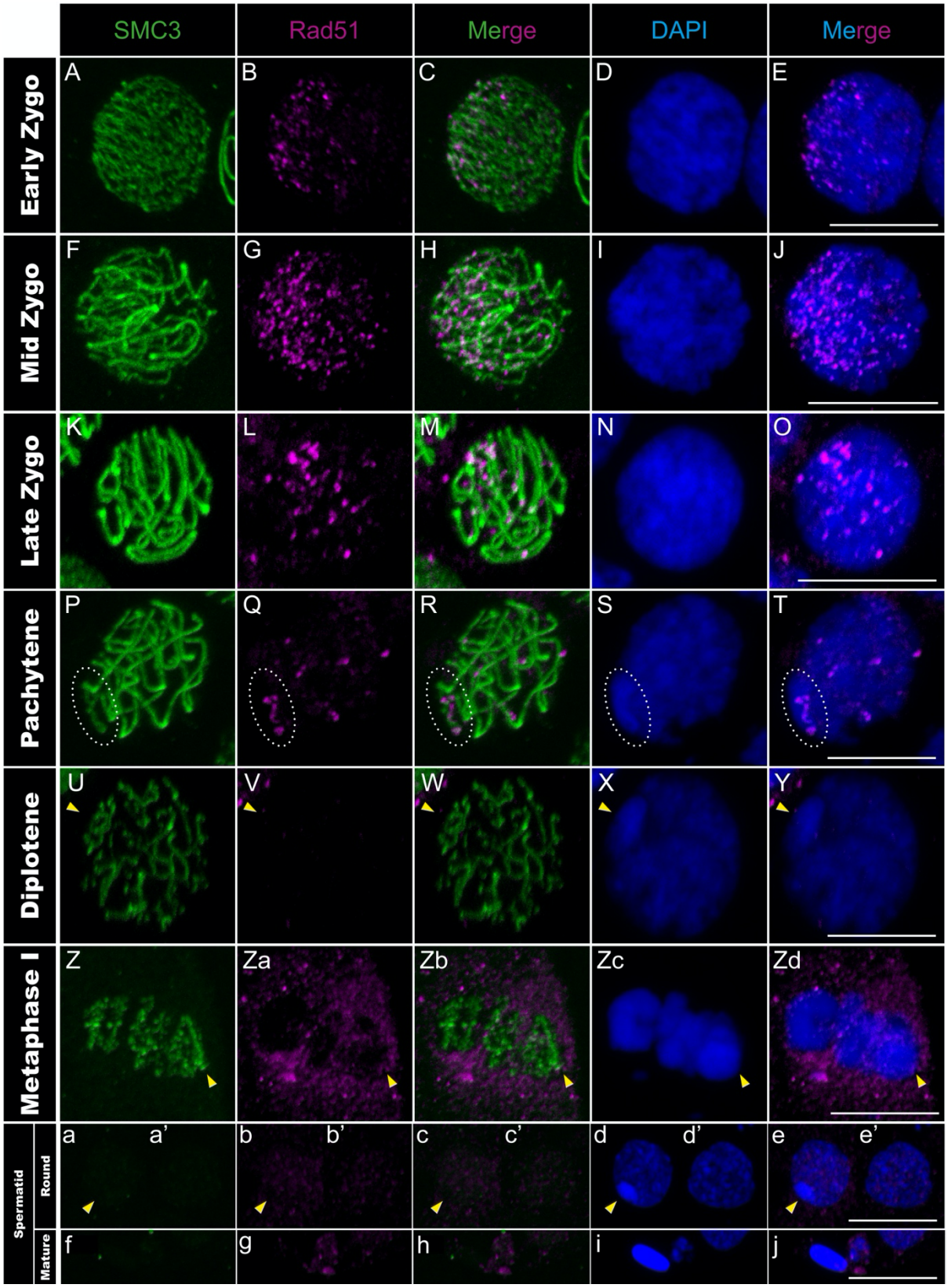

Figure 2: Rad51 distribution in *T. californicum* meiocytes and spermatids. Projections of stack images acquired across *T. californicum* squashed meiocytes (A–Zd) and spermatids (a–o), at the stages indicated, stained with DAPI (blue) and double immunolabeled for SMC3 (green) and Rad51

630 (magenta). During the early to mid-zygotene transition, there is an increase in the number of Rad51
631 foci and a localisation in one nuclear pole, as for γH2AX. As synapsis progresses, the number of Rad51
632 foci decreases and a few remain on SMC3 axes in pachytene. An accumulation of Rad51 foci on the X
633 chromosome is also observed in pachytene. The position of the X chromosome is indicated with
634 arrowheads and the associated Rad51 signal along its SMC3 axis with dashed circles in pachytene.
635 Scale bar: 10 µm. See Supplementary figure 2 for screens in males of other *Timema* species.

636

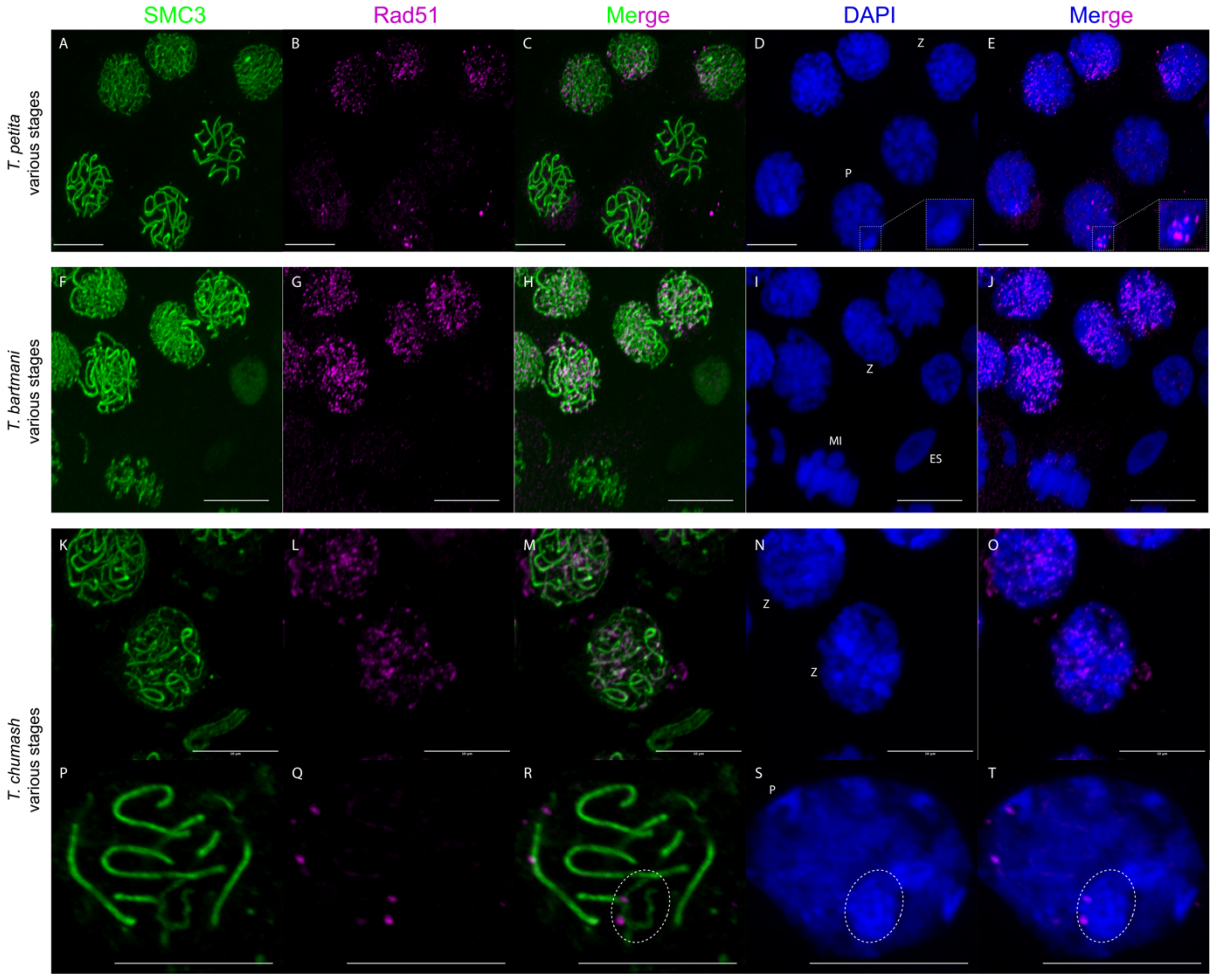

637

638 **Supplementary figure 2:** Rad51 distribution at various stages of spermatogenesis for three additional
639 *Timema* species, acquired through the projection of stack images. Focal cells at the zygotene stage are
640 labeled with the letter *Z*, cells at the pachytene stage with the letter *P*, cells in metaphase I with the
641 letters MI, and elongated spermatid cells with the letters ES. Inset zooms on the X chromosome in

642 pachytene are shown for *T. petita*, while in *T. chumash*, dashed circles indicate the position of the sex

643 (X) chromosome and the associated Rad51 signal along its SMC3 axis in pachytene. Scale bar: 10 µm.

644

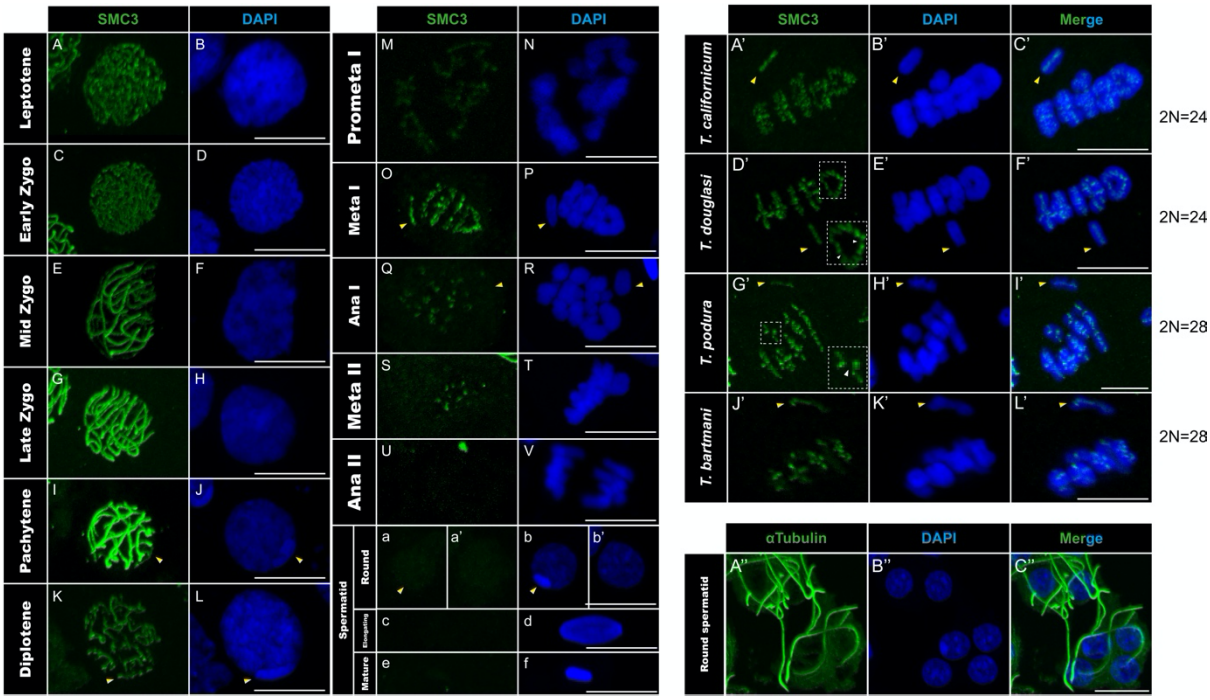

646 **Supplementary figure 3: Characterization of spermatogenetic stages and X chromosome**

647 **identification.** (A-f) illustrate SMC3 and DAPI stainings throughout *T. californicum* spermatogenesis.

648 While forming thin filaments along chromosomal axes at the onset of meiosis, SMC3 filaments appear

649 thicker as synapsis progresses between homologs (A-J). At metaphase I, SMC3 forms cross-shaped or

650 ring-shaped signals corresponding to rod and ring bivalents, respectively (O-P). As homologs segregate

651 during anaphase I, SMC3 concentrates into foci near centromeres until metaphase II (Q-T). SMC3 is

652 then lost from anaphase II onwards (U-f). Note that during the round spermatid stage, nullo-X and X-

653 containing spermatids are represented (a-b'). (A'-L') illustrate rod and ring bivalents across 4 *Timema*

654 species at metaphase I. Dashed squares indicate zooms of individual chromosomes illustrating rod and

655 ring bivalents with interrupted SMC3 signal near chromosomal ends (white arrowheads in D' and G').

656 Note that across many metaphases I analyzed, we observed consistent formation of a single, large

657 "ring" bivalent in *T. californicum* and *T. douglasi* but not in *T. podura* and *T. bartmani*. (A''-C'') illustrate

658 the formation of the flagellum during spermiogenesis as evidenced by α-tubulin staining in round
659 spermatids. The position of the X chromosome is indicated with yellow arrowheads. Scale bar: 10 µm.
660

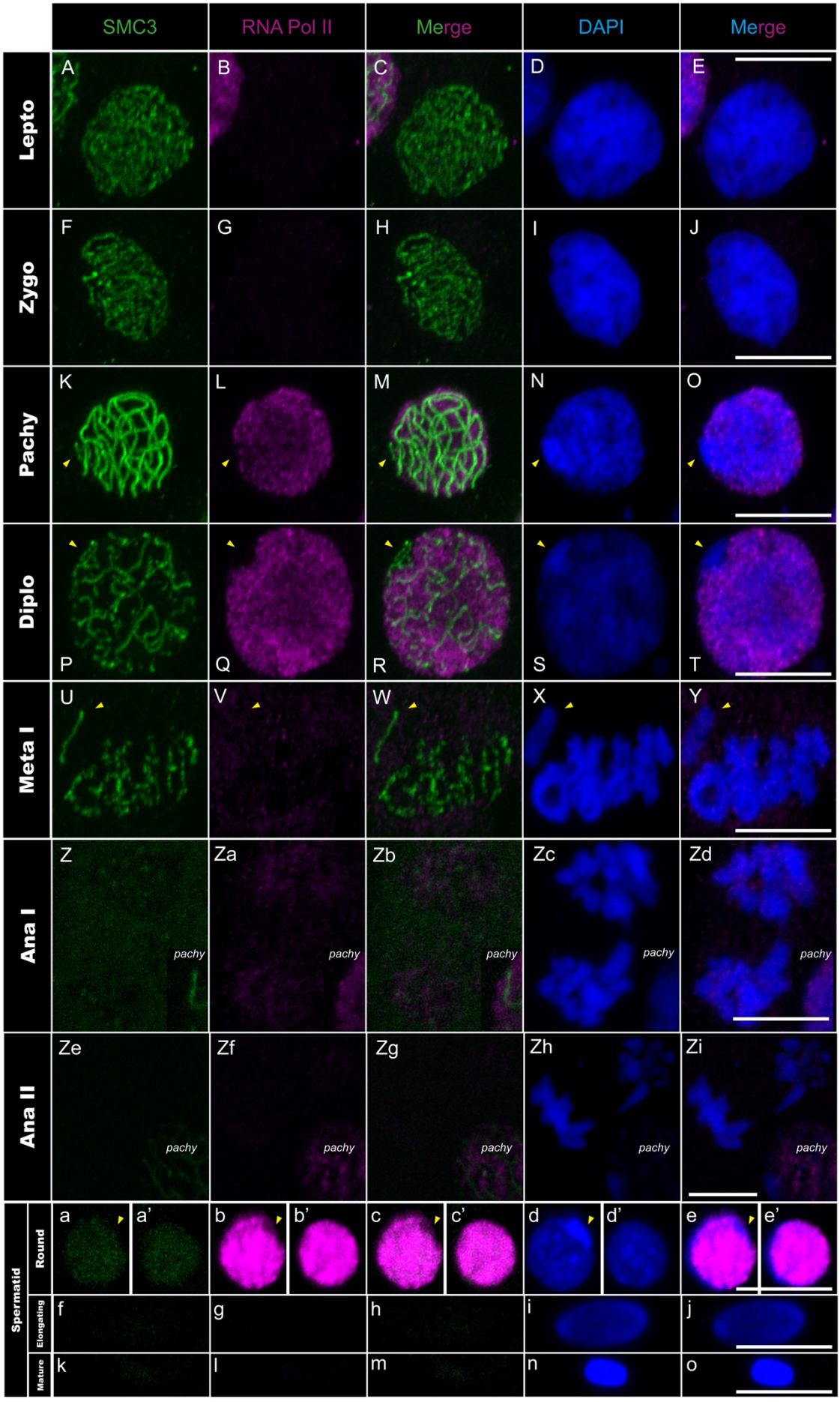
SMC3
RNA Pol II
Merge
DAPI
Merge
Lepto
Zygo
Pachy
Diplo
Meta I
Ana I
Ana II
Spermatid
Round
Elongating
Mature
A
B
C
D
E
F
G
H
I
J
K
L
M
N
O
P
Q
R
S
T
U
V
W
X
Y
Z
Za
Zb
Zc
Zd
Ze
Zf
Zg
Zh
Zi
pachy
a
a'
b
b'
c
c'
d
d'
e
e'
f
g
h
i
j
k
l
m
n
o

661

662 **Figure 3:** RNApol-II distribution in *T. californicum* meiocytes and spermatids. Projections of stack
663 images acquired across *T. californicum* squashed meiocytes (A–Zi) and spermatids (a–o), at the stages
664 indicated, stained with DAPI (blue) and double immunolabeled for SMC3 (green) and RNApol-II
665 (magenta). RNApol-II labeling is intense from pachytene to diplotene, and in the round spermatid
666 stage. During all spermatogenesis stages, the X chromosome is extremely reduced in RNApol-II
667 labeling. The position of the X chromosome is indicated with arrowheads. Scale bar: 10 µm.
668

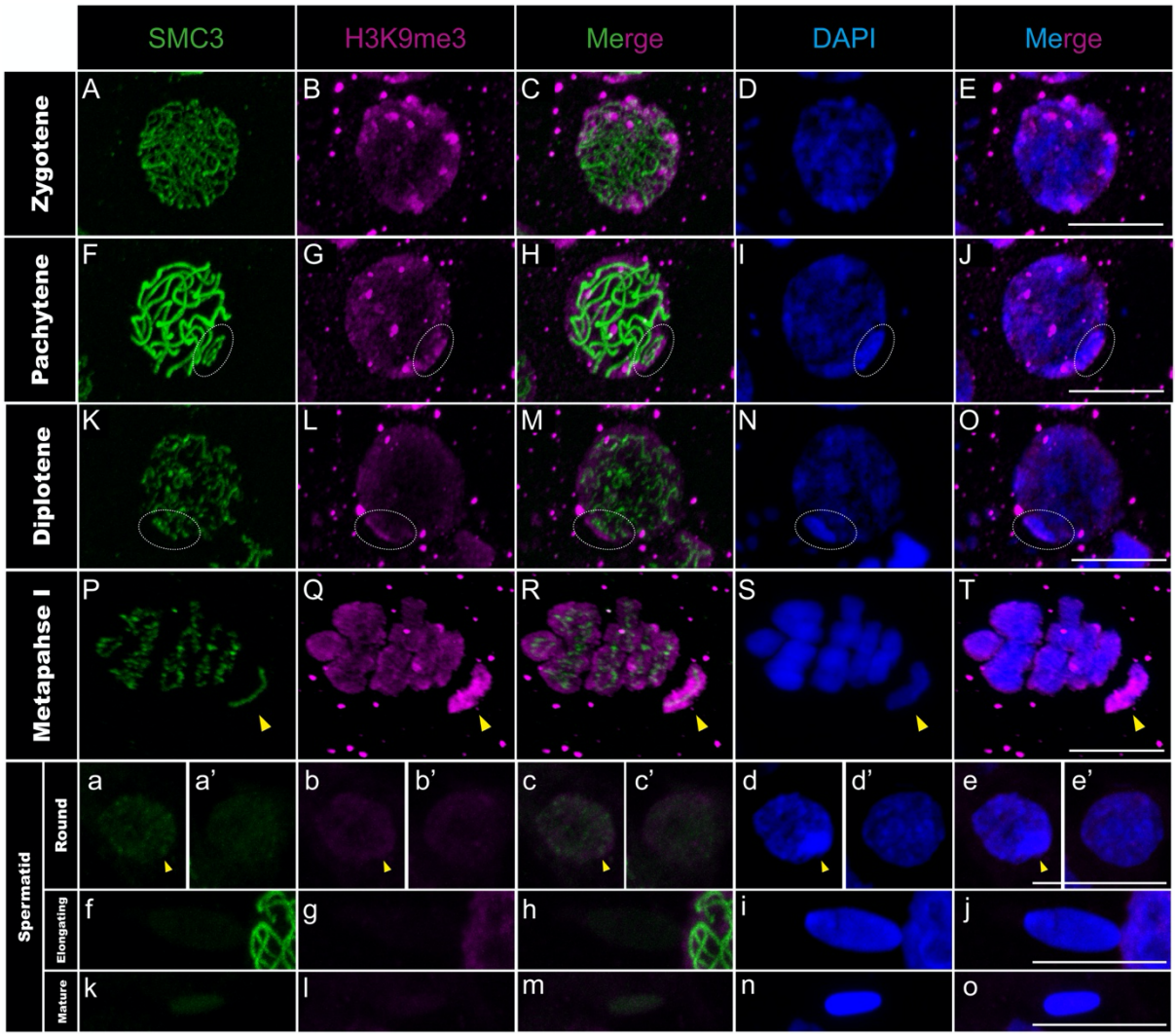

669

670 **Figure 4:** H3K9me3 distribution in *T. californicum* meiocytes. Projections of stack images acquired
671 across *T. californicum* squashed meiocytes (A–T) and spermatids (a–o), at the stages indicated, stained
672 with DAPI (blue) and double immunolabeled for SMC3 (green) and H3K9me3 (magenta). H3K9me3
673 labeling is particularly intense, coating the X chromosome from the pachytene stage. During

674 spermiogenesis, H3K9me3 signal is absent on the X chromosome. The position of the X chromosome
675 and the associated H3K9me3 signal is indicated with dashed circles in pachytene/diplotene and with
676 arrowheads in metaphase I/round spermatids. Scale bar: 10 µm. See Supplementary figure 4 for
677 screens in males of other *Timema* species.

678

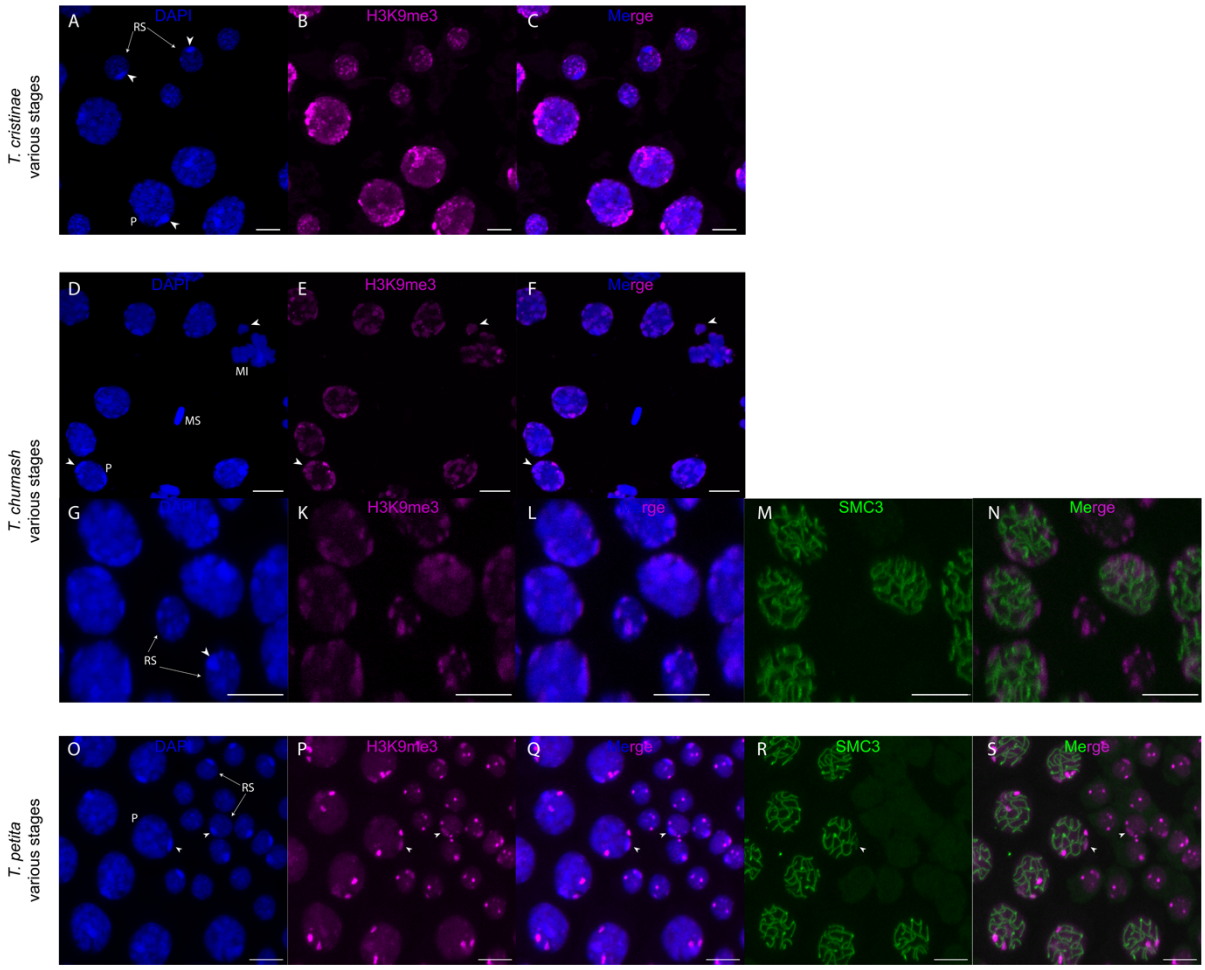

679

680 **Supplementary figure 4:** H3K9me3 distribution at various stages of spermatogenesis for three
681 additional *Timema* species, acquired through the projection of stack images. Focal cells at the
682 pachytene stage are labeled with the letter *P*, cells in metaphase I with the letters MI, round spermatid
683 cells with the letters RS, and mature sperm cells with the letters MS. Note the presence of H3K9me3
684 coating the X chromosome in round spermatids in *T. petita* and *T. chumash* but not in *T. cristinae*.
685 Arrowheads indicate the location of the X chromosome. Scale bar: 10 µm.

686

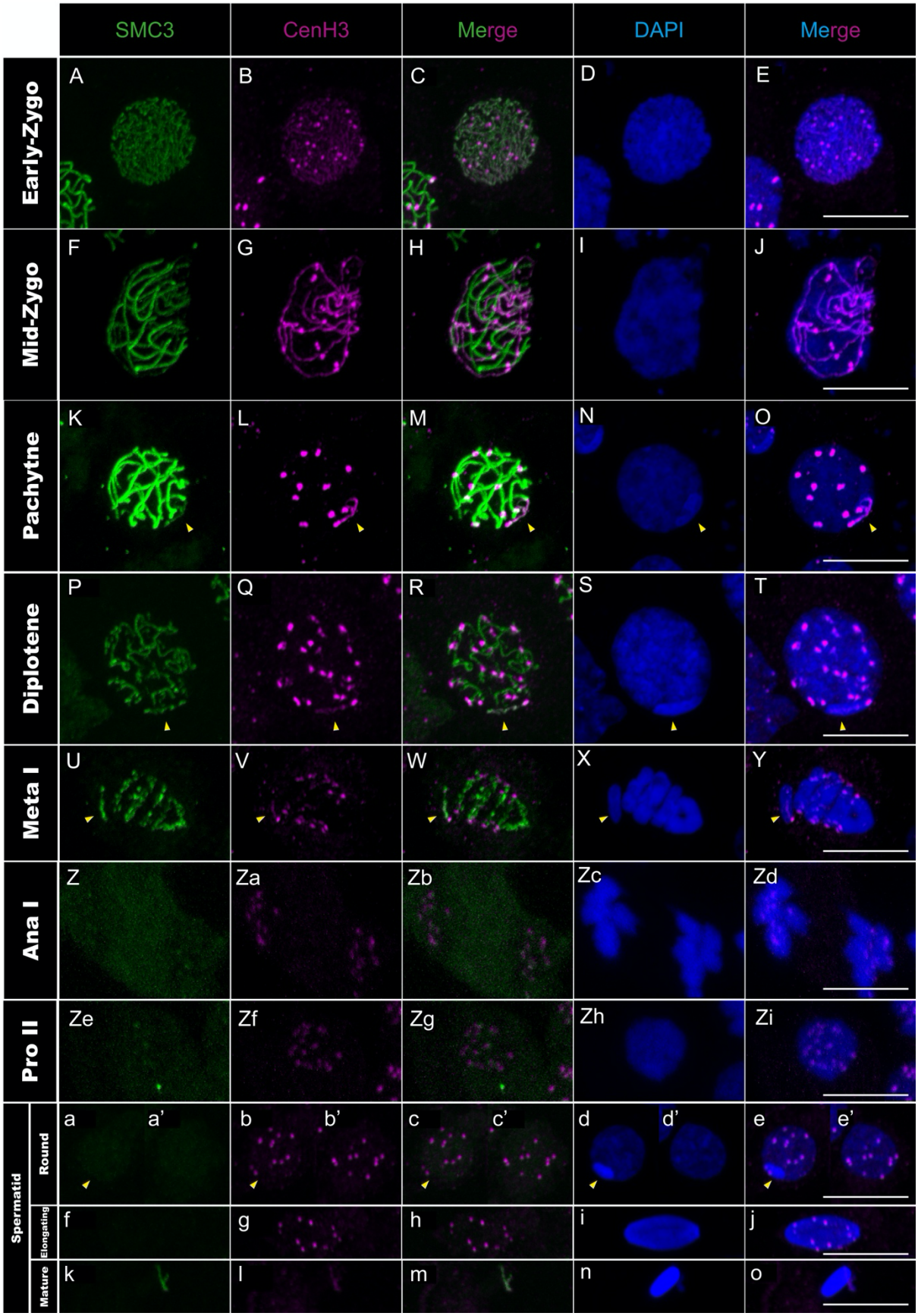
SMC3
CenH3
Merge
DAPI
Merge
Early-Zygo
Mid-Zygo
Pachytne
Diplotene
Meta I
Ana I
Pro II
Spermatid
Round
Elongating
Mature
A
B
C
D
E
F
G
H
I
J
K
L
M
N
O
P
Q
R
S
T
U
V
W
X
Y
Z
Za
Zb
Zc
Zd
Ze
Zf
Zg
Zh
Zi
a
a'
b
b'
c
c'
d
d'
e
e'
f
g
h
i
j
k
l
m
n
o

687

688 **Figure 5:** CenH3 distribution in *T. californicum* meiocytes and spermatids. Projections of stack images
689 acquired across *T. californicum* squashed meiocytes (A–Zi) and spermatids (a–o), at the stages
690 indicated, stained with DAPI (blue) and double immunolabeled for SMC3 (green) and CenH3
691 (magenta). While CenH3 is distributed along chromosomal axes at the onset of meiosis (early
692 zygotene), it becomes restricted to foci, first in autosomes as synapsis progresses (from mid-zygotene
693 to metaphase I), then also in X chromosome from anaphase I. The position of the X chromosome is
694 indicated with arrowheads. Scale bar: 10 µm. See Supplementary figure 7 for screens in males of other
695 *Timema* species.
696

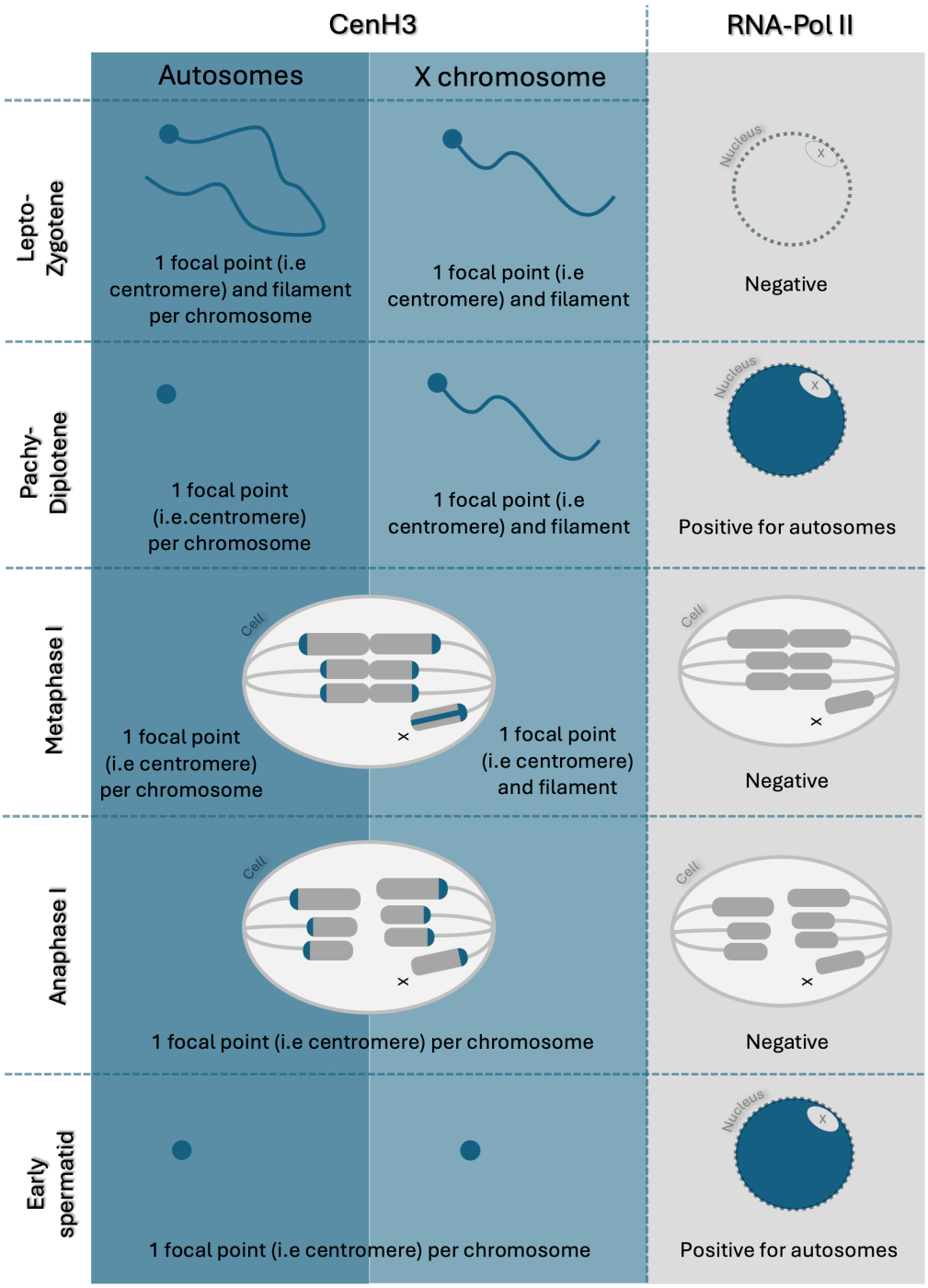

Supplementary figure 5: Schematic representation of CenH3 and RNApol-II distributions across different stages of spermatogenesis in *Timema*. The first activation of transcription in autosomes coinsides with the shift from a longitudinal to a focal distribution of CenH3 along these same chromosomes. However, the shift of CenH3 along the X chromosome is not associated with its transcriptional activation in anaphase I. Scale bar: 10 µm.

703

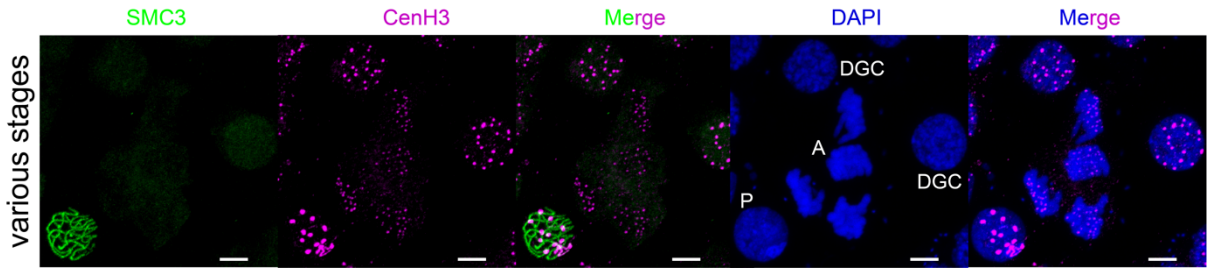

704

705 **Supplementary figure 6:** CenH3 distribution in germ cells of *T. californicum* male gonads, stained with

706 DAPI (blue) and double immunolabeled for SMC3 (green) and CenH3 (magenta). The acquisition

707 contrasts the distribution of CenH3 for cells in meiosis ("P" for Pachytene) and before entering meiosis

708 ("DGC" for Diploid Germ Cell and "A" for Anaphase). Scale bar: 5 µm.

709

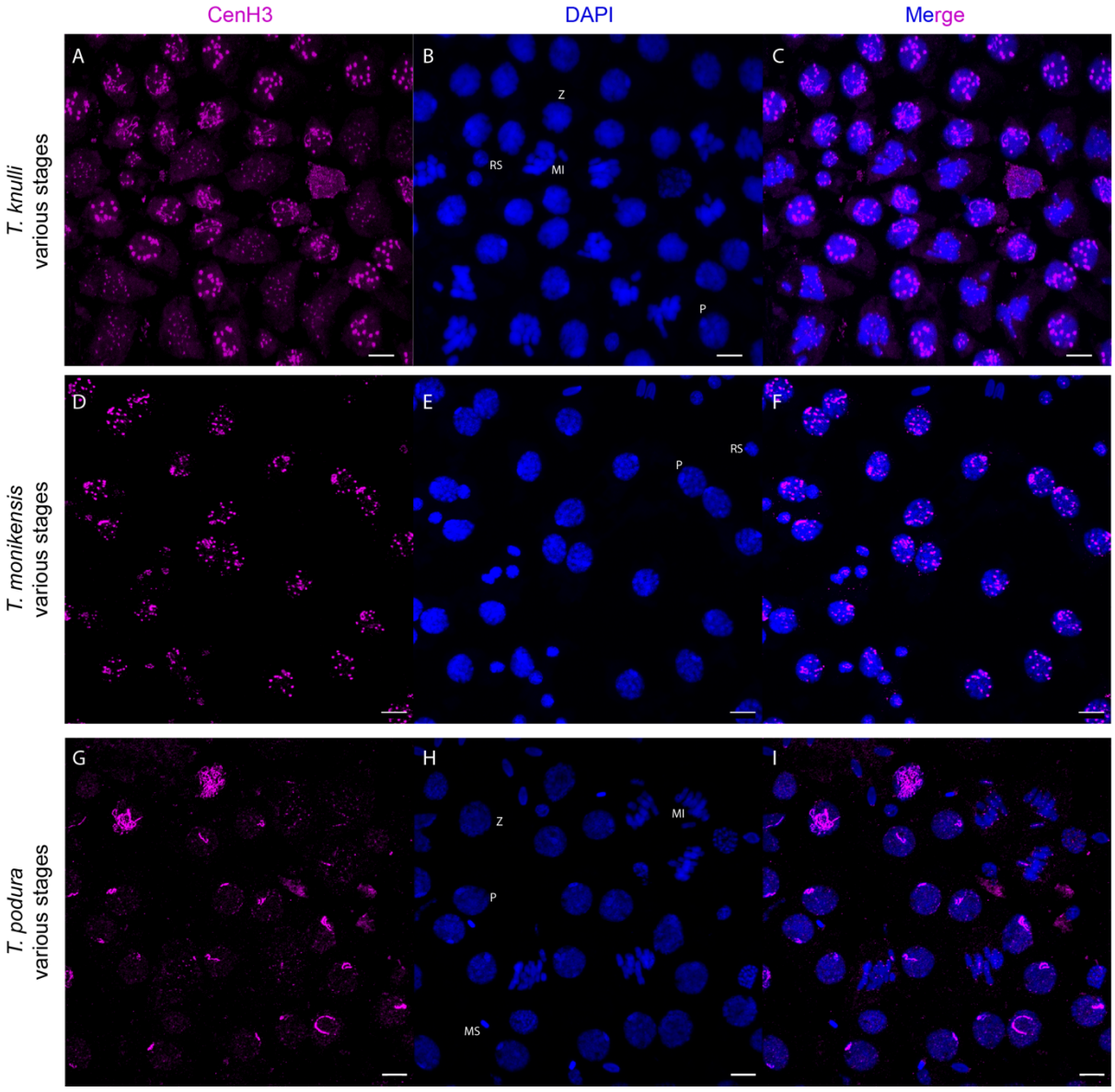

710

711 **Supplementary figure 7:** Projections of stack images acquired across various stages of

712 spermatogenesis for three additional species, stained with DAPI (blue) and immunolabeled for CenH3

713 (magenta). Focal cells in zygotene are labeled with letter Z, cells at the pachytene stage with the letter

714 *P*, cells in metaphase I with the letters MI, round spermatid cells with the letters RS, and mature sperm

715 cells with the letters MS. Scale bar: 10 µm.

716

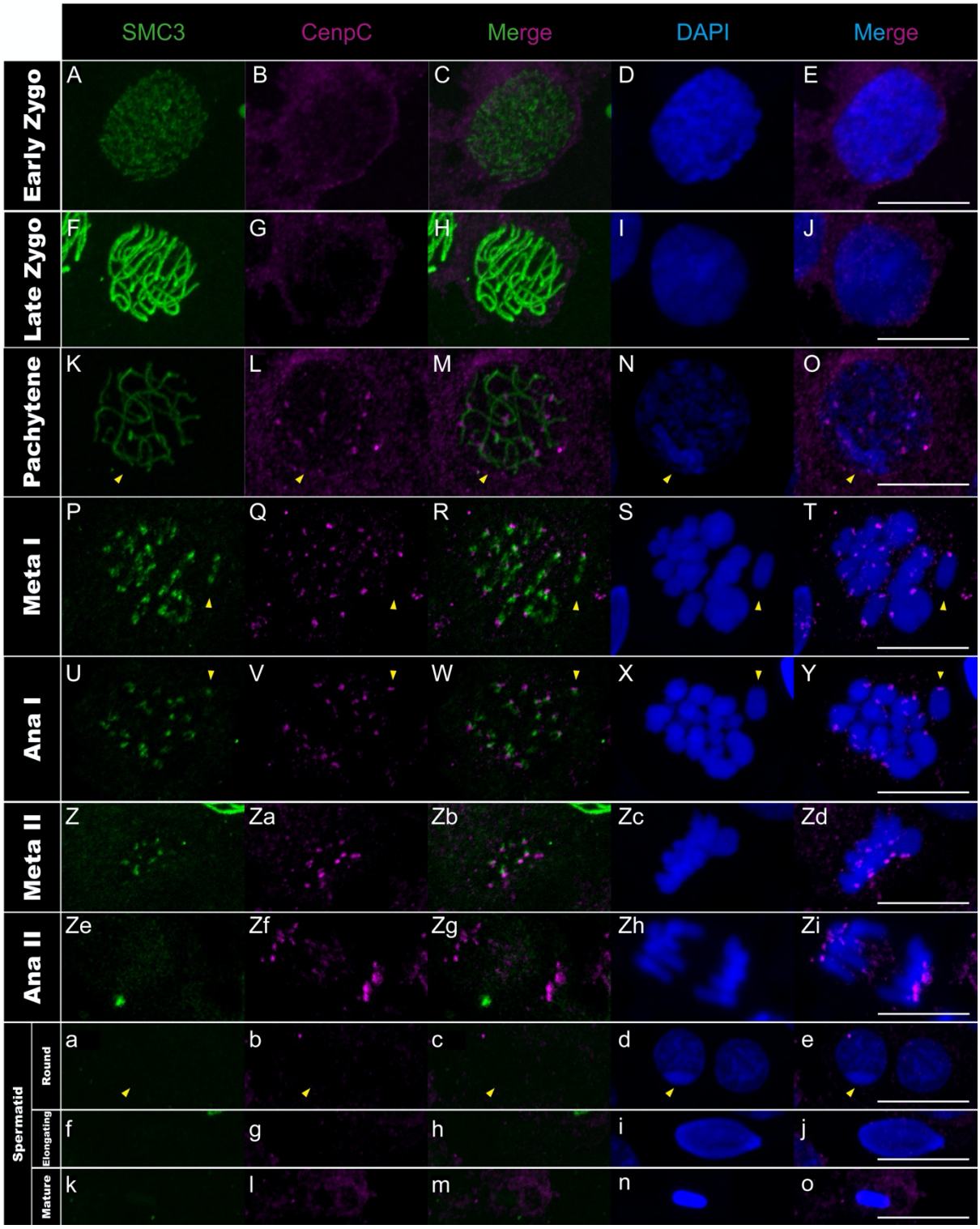

Figure 6: CenpC distribution in *T. californicum* meiocytes and spermatids. Projections of stack images acquired across *T. californicum* squashed meiocytes (A–Zi) and spermatids (a–o), at the stages indicated, stained with DAPI (blue) and double immunolabeled for SMC3 (green) and CenpC (magenta). The CenpC signal is not detected until the pachytene stage where it is distributed in foci

722 on every chromosome until anaphase II. The CenpC signal is then lost at the onset of spermiogenesis.

723 The position of the X chromosome is indicated with arrowheads. Scale bar: 10 µm.

724

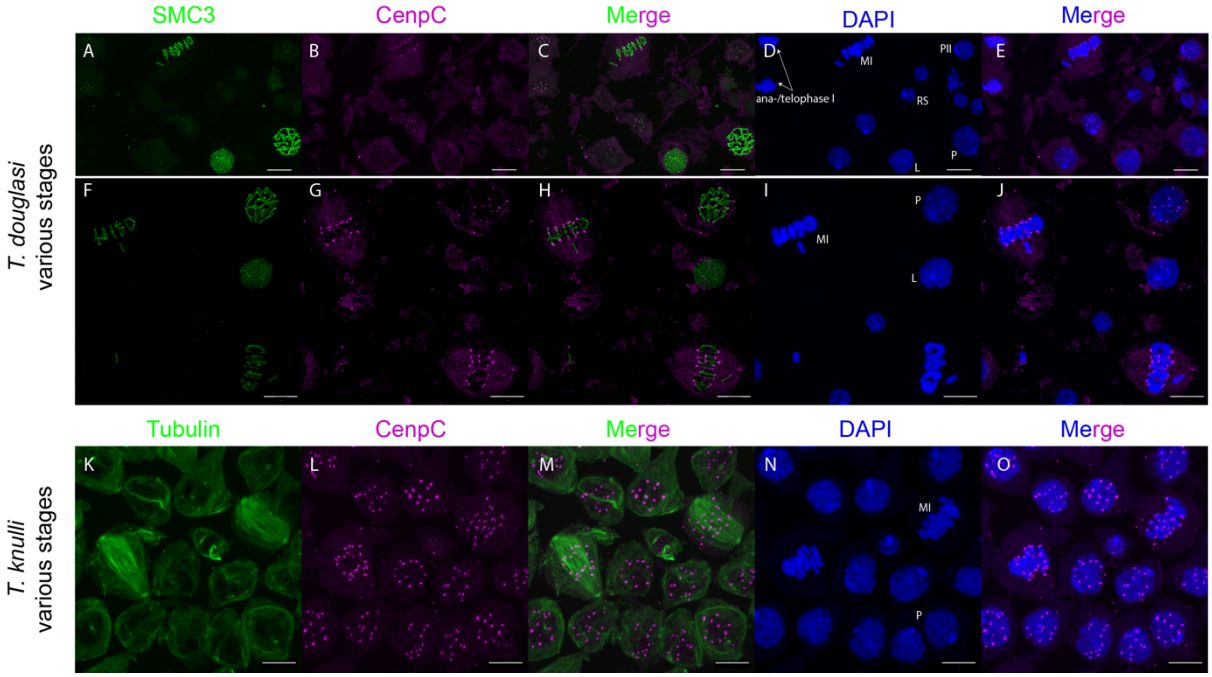

725

726 **Supplementary figure 8:** CenpC distribution at various stages of spermatogenesis for two additional

727 species, acquired through the projection of stack images. Focal cells in leptotene are labeled with the

728 letter L, cells at the pachytene stage with the letter *P*, cells in metaphase I with the letters MI, cells in

729 prophase II with the letters PII, and round spermatid cells with the letters RS. Note that the lower

730 signal intensity in the upper panel is caused by a different objective and does not reflect species

731 variation. Scale bar: 10 µm.

732

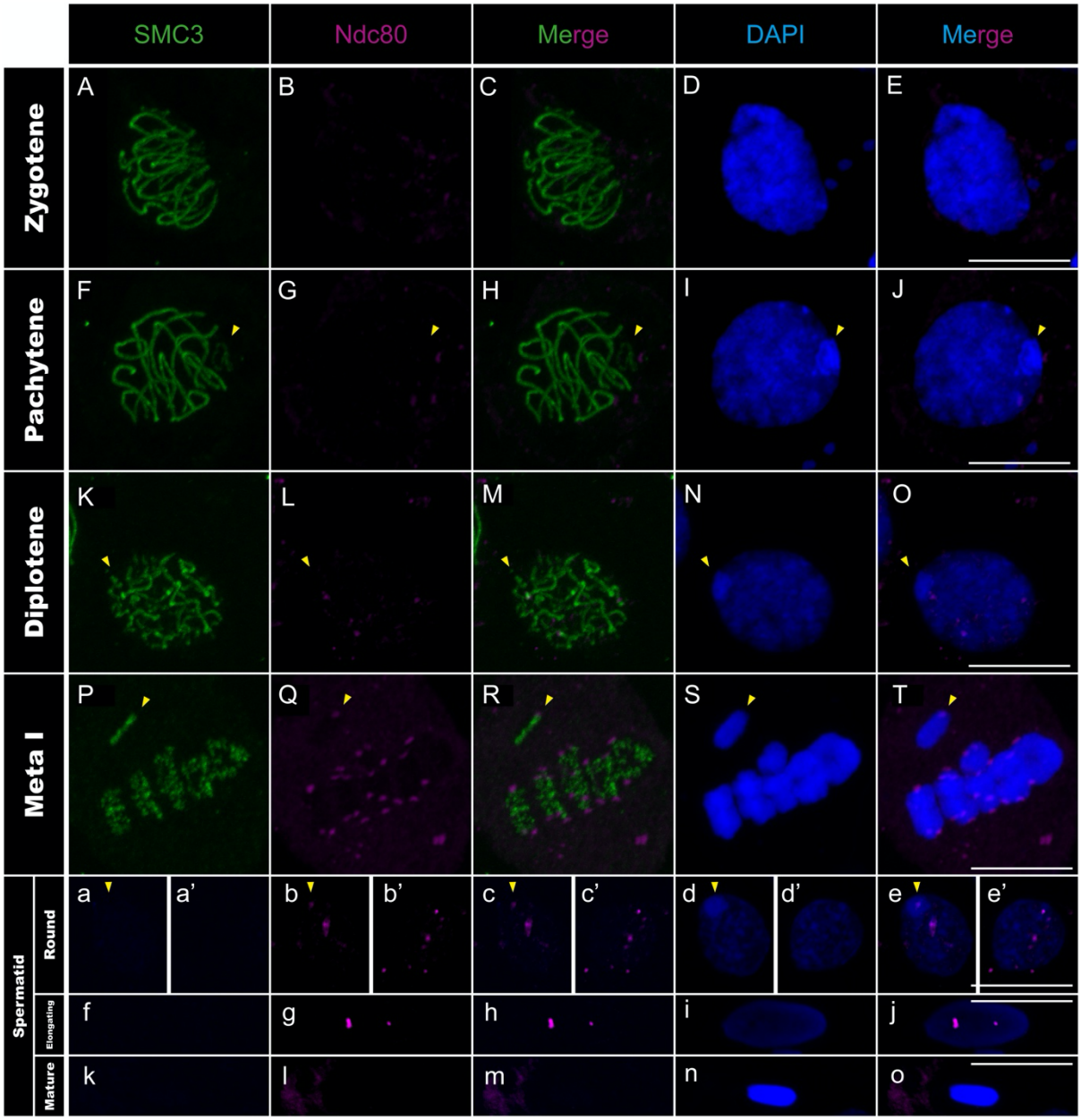

Figure 7: Ndc80 distribution in *T. californicum* meiocytes and spermatids. Projections of stack images acquired across *T. californicum* squashed meiocytes (A–T) and spermatids (a–o), at the stages indicated, stained with DAPI (blue) and double immunolabeled for SMC3 (green) and Ndc80 (magenta). Ndc80 signal is not detected until the pro-metaphase I stage (see Supplemental figure 9) where it is distributed in a single focus on all chromosomes until anaphase II (see Supplemental figure 9). The Ndc80 signal is then lost from centromeres at the onset of spermiogenesis, although two to three regions (likely non-centromeric, see main text) appear positive for Ndc80 in round and

741 elongated spermatids. The position of the X chromosome is indicated with arrowheads. Scale bar: 10

742 µm.

743

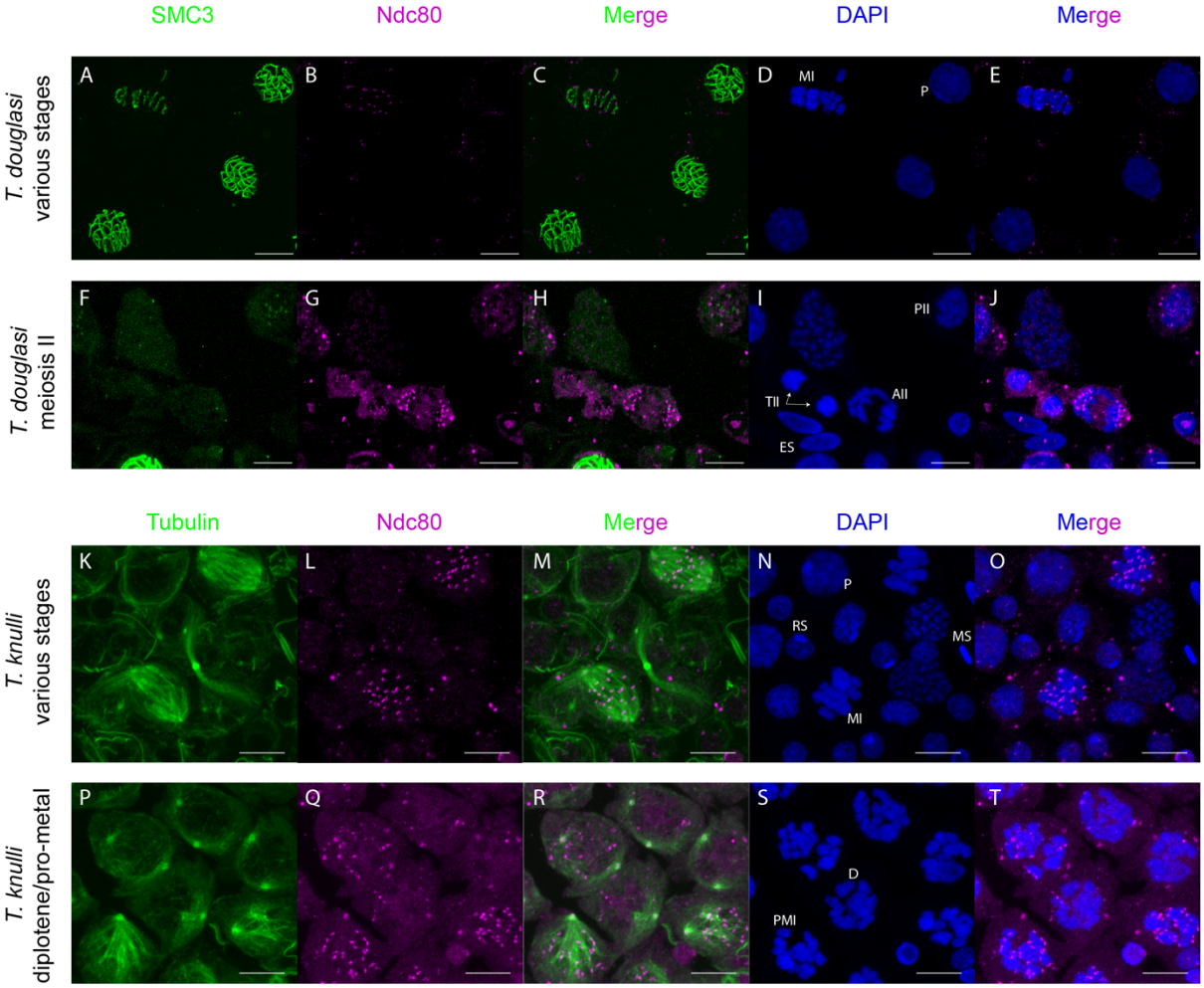

744

745 **Supplementary figure 9:** Ndc80 distribution in various stages of spermatogenesis for two additional

746 species, acquired through the projection of stack images. Focal cells at the pachytene stage are labeled

747 with the letter *P*, cells in diplotene with the letter D, cells in pro-metaphase I with letters PMI, cells in

748 metaphase I with the letters MI, cells in prophase II with the letters PII, cells in anaphase II with letters

749 AII, cells in telophase II with letters TII, round spermatid cells with the letters RS, elongated spermatid

750 cells with letters ES, and mature sperm cells with letters RS. Note that at the diplotene stage,

751 chromosomes are already condensed but spindle microtubules (immunolabeled with α-tubulin) are

752 not yet polymerized as compared to the pro-metaphase I stage. Scale bar: 10 µm.

753

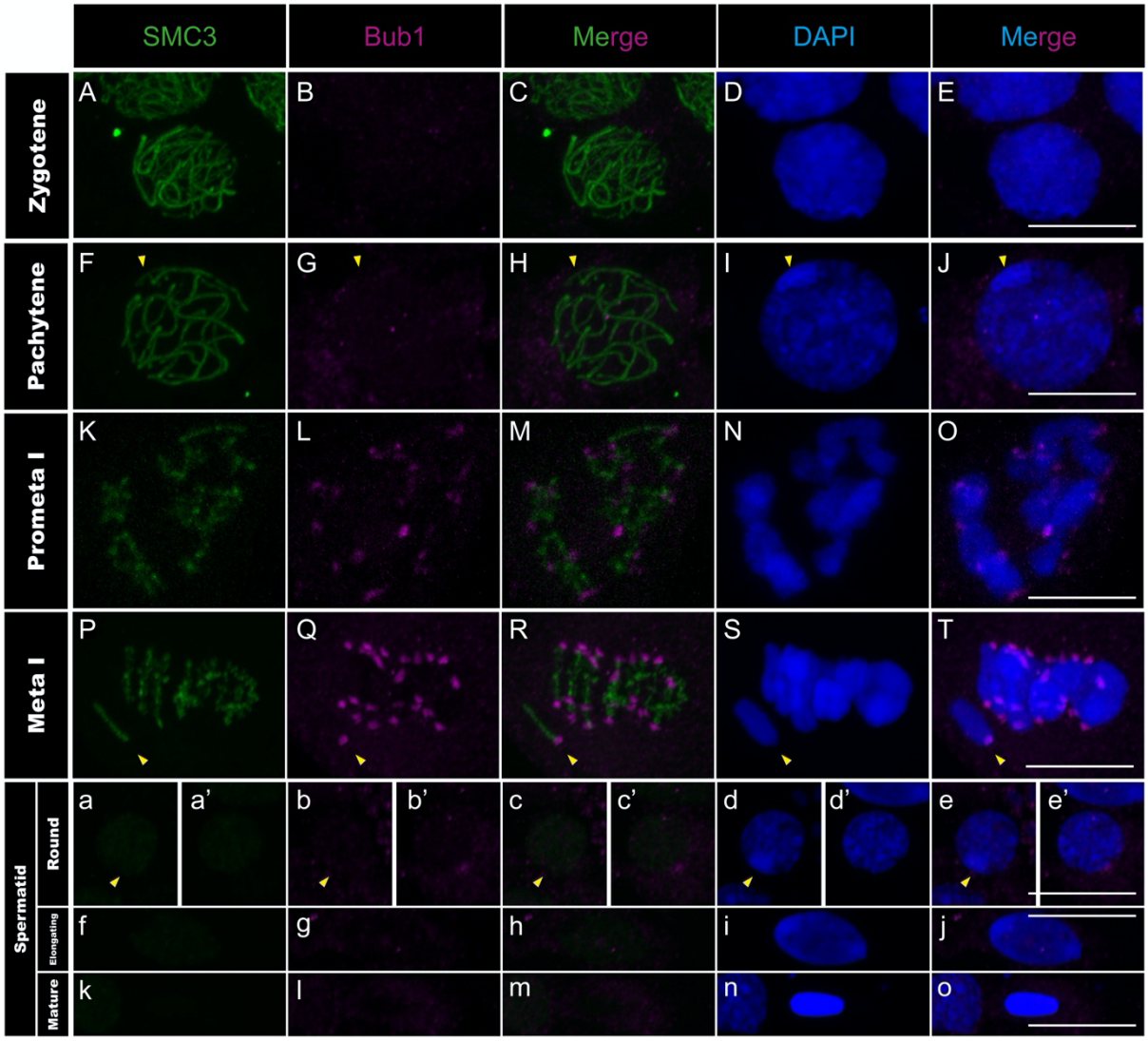

754

755 **Figure 8:** Bub1 distribution in *T. californicum* meiocytes and spermatids. Projections of stack images

756 acquired across *T. californicum* squashed meiocytes (A–T) and spermatids (a–o), in the stages

757 indicated, stained with DAPI (blue) and double immunolabeled for SMC3 (green) and Bub1 (magenta).

758 Bub1 signal is not detected until the pro-metaphase I stage where it is distributed in foci on every

759 chromosome until the second meiotic division (see Supplemental figure 10). The Bub1 signal is then

760 lost during spermiogenesis. The position of the X chromosome is indicated with arrowheads. Scale

761 bar: 10 µm.

762

763 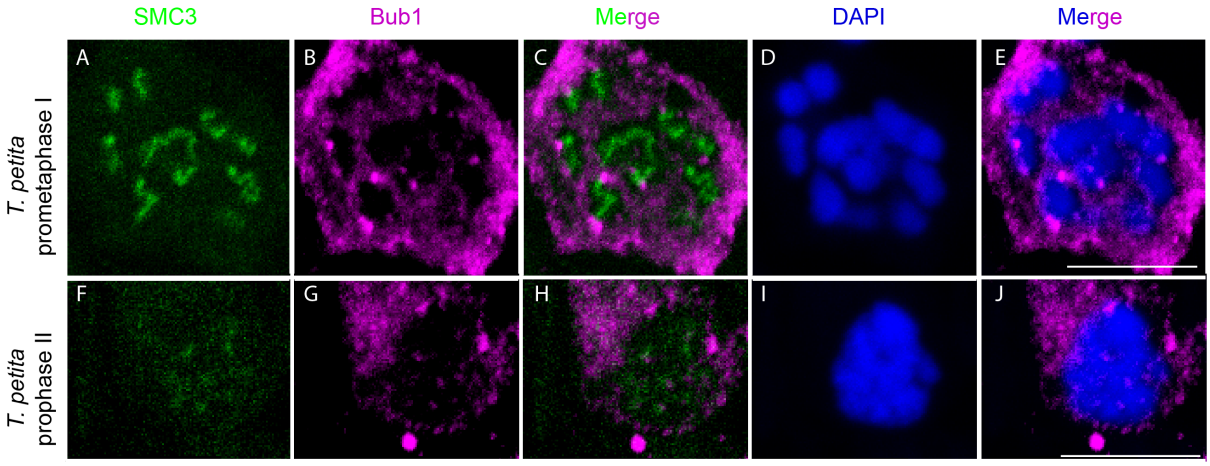

764 **Supplementary figure 10:** Bub1 distribution at prometaphase I and prophase II stages in *T. petita*,

765 acquired through the projection of stack images. Scale bar: 10 µm.

766

Species	Specimen	γH2AX at zygotene	γH2AX at pachytene on X
T. califonicum	A*	Cloud of foci at one nuclear pole	Positive
	B	Cloud of foci at one nuclear pole	Positive
	C	Cloud of foci at one nuclear pole	Positive
T. petita	A**	Cloud of foci at one nuclear pole	Positive
T. cristinae	A**	Cloud of foci at one nuclear pole	Negative
	B	Cloud of foci at one nuclear pole	Negative
T. chumach	A**	Cloud of foci at one nuclear pole	Negative
	B	Cloud of foci at one nuclear pole	Negative

* See Figure 1

** See Supplemental figure 1

767

768 **Supplementary table 1:** γH2AX distribution across species and individuals during the zygotene

769 (bouquet) stage as well as on the X chromosome during pachytene (i.e., the initiation of

770 MSCI).

771

List of primary custom antibodies

Short Name	Company	Clonality	Host	Peptide sequence
Bub1	Covalab	Polyclonal	Rabbit	C-EADNPIVYQELIKEQQRYE-coNH2 C-EFSLEELRAIIYNKKYEEK-coNH2 C-HPAIPSRPEEKSGPLQPST-coNH2
CenH3 (see (24) for details)				
CenpC (see (24) for details)				
Ndc80 (see (24) for details)				

List of primary commercial antibodies

Short Name	Ref	Company	Final Concentration	Conjugated/Host
SMC3	ab201542	AbCam	1:100	Alexa Fluor 488/Rabbit
RNA Pol II	ab193468	AbCam	1:100	No/Rabbit
H3K9me3	ab8898	AbCam	1:100	No/Rabbit
RAD51	PC130	Sigma-Aldrich	1:70	No/Rabbit
γH2AX	05-636	Sigma-Aldrich	1:200	No/Rabbit
α_Tubulin	#F2168	Sigma-Aldrich	1:150	FITC/Mouse

List of secondary antibodies

Short Name	Ref	Company	Final Concentration	Conjugated
anti-Rabbit-Alexa 594	711-585-152	Jackson	1:150	Alexa Fluor 594

Chemicals used for immuno-staining

Name	Ref	Company	Working Solution
DAPI	D9542	Sigma-Aldrich	10ug/mL
Normal Rabbit Serum (NRS)	X090210-8	Agilent Technonoly	5% in PBS 1x (v/v)
Vectashield Mounting Medium	H1000	ReactoLab	

Supplementary table 2: Antibodies and chemicals used. A combination of custom and commercially available antibodies were employed for the immunostaining assays.

Species	γH2AX	Rad51	RNA Polymerase II	H3K9me3	CenH3	CenpC	Ndc80	Bub1
T. califonicum	3 individuals	3 individuals	1 individual	2 individuals	3 individuals	3 individuals	2 individuals	1 individual
T. popensis			1 individual					
T. douglasi					3 individuals	2 individuals	2 individuals	
T. petita	1 individual	1 individual		1 individual	2 individuals			1 individual
T. knulli					1 individual	1 individual	1 individual	
T. monikensis					1 individual			
T. cristinae	1 individual			2 individuals				
T. bartmani		1 individual						
T. podura					2 individuals			
T. chumach	2 individuals	1 individual		2 individuals				

Supplementary table 3: Inter- and intra-species replication of the cellular patterns described in this study as well as in (24, 25).

784 REFERENCES

785

786 1. Zickler D, Kleckner N. Meiosis: Dances Between Homologs. Annu Rev Genet.
787 2023;57:1-63.
788 2. Hao SL, Ni FD, Yang WX. The dynamics and regulation of chromatin remodeling during
789 spermiogenesis. Gene. 2019;706:201-10.
790 3. Lenormand T, Engelstädter J, Johnston SE, Wijnker E, Haag CR. Evolutionary mysteries
791 in meiosis. Philos T R Soc B. 2016;371(1706).
792 4. Loidl J. Conservation and Variability of Meiosis Across the Eukaryotes. Annual Review
793 of Genetics, Vol 50. 2016;50:293-316.
794 5. White-Cooper H, Bausek N. Evolution and spermatogenesis. Philos T R Soc B.
795 2010;365(1546):1465-80.
796 6. Gerton JL, Hawley RS. Homologous chromosome interactions in meiosis: Diversity
797 amidst conservation. Nat Rev Genet. 2005;6(6):477-87.
798 7. T. SKONE. Achiasmy and sex chromosome evolution. Ecological Genetics and
799 Genomics. 2019.
800 8. Jang JK, Sherizen DE, Bhagat R, Manheim EA, McKim KS. Relationship of DNA double-
801 strand breaks to synapsis in Drosophila. J Cell Sci. 2003;116(15):3069-77.
802 9. Viera A, Santos JL, Page J, Parra MT, Calvente A, Cifuentes M, et al. DNA double-strand
803 breaks, recombination and synapsis:: the timing of meiosis differs in grasshoppers and flies.
804 Embo Rep. 2004;5(4):385-91.
805 10. Page J, de la Fuente R, Gómez R, Calvente A, Viera A, Parra MT, et al. Sex
806 chromosomes, synapsis, and cohesins: a complex affair. Chromosoma. 2006;115(3):250-9.
807 11. Turner JMA. Meiotic sex chromosome inactivation. Development. 2007;134(10):1823-
808 31.
809 12. Daish TJ, Casey AE, Grutzner F. Lack of sex chromosome specific meiotic silencing in
810 platypus reveals origin of MSCI in therian mammals. Bmc Biol. 2015;13.
811 13. Guioli S, Lovell-Badge R, Turner JMA. Error-Prone ZW Pairing and No Evidence for
812 Meiotic Sex Chromosome Inactivation in the Chicken Germ Line. Plos Genet. 2012;8(3).
813 14. Namekawa SH, VandeBerg JL, McCarrey JR, Lee JT. Sex chromosome silencing in the
814 marsupial male germ line. P Natl Acad Sci USA. 2007;104(23):9730-5.
815 15. Page J, de la Fuente R, Manterola M, Parra MT, Viera A, Berríos S, et al. Inactivation or
816 non-reactivation: what accounts better for the silence of sex chromosomes during
817 mammalian male meiosis? Chromosoma. 2012;121(3):307-26.
818 16. Viera A, Parra MT, Arevalo S, de la Vega CG, Santos JL, Page J. X Chromosome
819 Inactivation during Grasshopper Spermatogenesis. Genes-Basel. 2021;12(12).
820 17. Cloutier JM, Turner JMA. Meiotic sex chromosome inactivation. Curr Biol.
821 2010;20(22):R962-R3.
822 18. McKinley KL, Cheeseman IM. The molecular basis for centromere identity and
823 function. Nat Rev Mol Cell Bio. 2016;17(1).
824 19. Mellone BG, Fachinetti D. Diverse mechanisms of centromere specification. Curr Biol.
825 2021;31(22):R1491-R504.
826 20. Cleveland DW, Mao YH, Sullivan KF. Centromeres and kinetochores: From epigenetics
827 to mitotic checkpoint signaling. Cell. 2003;112(4):407-21.
828 21. Senaratne AP, Cortes-Silva N, Drinnenberg IA. Evolution of holocentric chromosomes:
829 Drivers, diversity, and deterrents. Semin Cell Dev Biol. 2022;127:90-9.

22. Neumann P, Oliveira L, Jang TS, Novák P, Koblizková A, Schubert V, et al. Disruption of the standard kinetochore in holocentric Cuscuta species. P Natl Acad Sci USA. 2023;120(21).
23. Kitaoka M, Yamashita YM. Running the gauntlet: challenges to genome integrity in spermiogenesis. Nucleus-Phila. 2024;15(1).
24. Djordjevic J, Tran Van P, Toubiana W, Labédan M, Dumas Z, Aury J, et al. Dynamics of X chromosome hyper-expression and inactivation in male tissues during stick insect development. Plos Genet. 2025;21(3).
25. Toubiana W, Dumas Z, Tran Van P, Parker DJ, Mérel V, Schubert V, et al. Functional monocentricity with holocentric characteristics and chromosome-specific centromeres in a stick insect. Sci Adv. 2025;11(1).
26. Riesch R, Muschick M, Lindtke D, Villoutreix R, Comeault AA, Farkas TE, et al. Transitions between phases of genomic differentiation during stick-insect speciation. Nat Ecol Evol. 2017;1(4).
27. Brown MS, Bishop DK. DNA Strand Exchange and RecA Homologs in Meiosis. Csh Perspect Biol. 2015;7(1).
28. Rogakou EP, Boon C, Redon C, Bonner WM. Megabase chromatin domains involved in DNA double-strand breaks in vivo. J Cell Biol. 1999;146(5):905-15.
29. Parker DJ, Jaron KS, Dumas Z, Robinson-Rechavi M, Schwander T. X chromosomes show relaxed selection and complete somatic dosage compensation across Timema stick insect species. J Evolution Biol. 2022;35(12).
30. Viera A, Santos JL, Parra MT, Calvente A, Gómez R, de la Fuente R, et al. Incomplete Synapsis and Chiasma Localization: The Chicken or the Egg? Cytogenet Genome Res. 2010;128(1-3):139-51.
31. Revenkova E, Jessberger R. Keeping sister chromatids together: cohesins in meiosis. Reproduction. 2005;130(6):783-90.
32. Scherthan H. A bouquet makes ends meet. Nat Rev Mol Cell Bio. 2001;2(8):621-7.
33. Miyazaki WY, Orrweaver TL. Sister-Chromatid Cohesion in Mitosis and Meiosis. Annu Rev Genet. 1994;28:167-87.
34. Mahadevaiah SK, Turner JMA, Baudat F, Rogakou EP, de Boer P, Blanco-Rodríguez J, et al. Recombinational DNA double-strand breaks in mice precede synapsis. Nat Genet. 2001;27(3):271-6.
35. Kleckner N. Meiosis: How could it work? P Natl Acad Sci USA. 1996;93(16):8167-74.
36. Grelon M, Vezon D, Gendrot G, Pelletier G. AtSPO11-1 is necessary for efficient meiotic recombination in plants. Embo J. 2001;20(3):589-600.
37. Munro C, Cadis H, Pagnotta S, Houliston E, Huynh JR. Conserved meiotic mechanisms in the cnidarian Clytia hemisphaerica revealed by Spo11 knockout. Sci Adv. 2023;9(4):eadd2873.
38. Schwander T, Crespi BJ. Multiple Direct Transitions from Sexual Reproduction to Apomictic Parthenogenesis in Stick Insects. Evolution. 2009;63(1):84-103.
39. Handel MA. The XY body: a specialized meiotic chromatin domain. Exp Cell Res. 2004;296(1):57-63.
40. Ichijima Y, Sin HS, Namekawa SH. Sex chromosome inactivation in germ cells: emerging roles of DNA damage response pathways. Cell Mol Life Sci. 2012;69(15):2559-72.
41. Viera A, Calvente A, Page J, Parra MT, Gómez R, Suja JA, et al. X and B chromosomes display similar meiotic characteristics in male grasshoppers. Cytogenet Genome Res. 2004;106(2-4):302-8.

876 42. Viera A, Parra MT, Rufas JS, Page J. Transcription reactivation during the first meiotic
877 prophase in bugs is not dependent on synapsis. Chromosoma. 2017;126(1):179-94.
878 43. Bowman EA, Kelly WG. RNA Polymerase II transcription elongation and Pol II CTD Ser2
879 phosphorylation A tail of two kinases. Nucleus-Phila. 2014;5(3):224-36.
880 44. Gorbsky GJ. The spindle checkpoint and chromosome segregation in meiosis. Febs J.
881 2015;282(13):2458-74.
882 45. Musacchio A, Desai A. A Molecular View of Kinetochore Assembly and Function.
883 Biology-Basel. 2017;6(1).
884 46. Musacchio A, Salmon ED. The spindle-assembly checkpoint in space and time. Nat Rev
885 Mol Cell Bio. 2007;8(5):379-93.
886 47. Chen JX, Ünal E. Meiotic regulation of the Ndc80 complex composition and function.
887 Curr Genet. 2021;67(4):511-8.
888 48. Miller MP, Ünal E, Brar GA, Amon A. Meiosis I chromosome segregation is established
889 through regulation of microtubule-kinetochore interactions. Elife. 2012;1.
890 49. Kursel LE, McConnell H, de la Cruz AFA, Malik HS. Gametic specialization of
891 centromeric histone paralogs in Drosophila virilis. Life Sci Alliance. 2021;4(7).
892 50. Gassmann R, Rechtsteiner A, Yuen KW, Muroyama A, Egelhofer T, Gaydos L, et al. An
893 inverse relationship to germline transcription defines centromeric chromatin in C. elegans.
894 Nature. 2012;484(7395):534-U166.
895 51. Li XT, Nicklas RB. Tension-sensitive kinetochore phosphorylation and the chromosome
896 distribution checkpoint in praying mantid spermatocytes. J Cell Sci. 1997;110:537-45.
897 52. Nicklas RB, Ward SC, Gorbsky GJ. Kinetochore Chemistry Is Sensitive to Tension and
898 May Link Mitotic Forces to a Cell-Cycle Checkpoint. J Cell Biol. 1995;130(4):929-39.
899 53. Nicklas RB, Waters JC, Salmon ED, Ward SC. Checkpoint signals in grasshopper meiosis
900 are sensitive to microtubule attachment, but tension is still essential. J Cell Sci.
901 2001;114(23):4173-83.
902 54. McKim KS, Hayashi-Hagihara A. Mei-W68 in Drosophila melanogaster encodes a
903 Spo11 homolog:: evidence that the mechanism for initiating meiotic recombination is
904 conserved. Gene Dev. 1998;12(18):2932-42.
905 55. Dernburg AF, McDonald K, Moulder G, Barstead R, Dresser M, Villeneuve AM. Meiotic
906 recombination in C. elegans initiates by a conserved mechanism and is dispensable for
907 homologous chromosome synapsis. Cell. 1998;94(3):387-98.
908 56. Viera A, Santos JL, Parra MT, Calvente A, Gómez R, de la Fuente R, et al. Cohesin axis
909 maturation and presence of RAD51 during first meiotic prophase in a true bug. Chromosoma.
910 2009;118(5):575-89.
911 57. Holm PB, Rasmussen SW. Chromosome-Pairing, Recombination Nodules and Chiasma
912 Formation in Diploid Bombyx Males. Carlsberg Res Commun. 1980;45(6):483-548.
913 58. Cahoon CK, Libuda DE. Leagues of their own: sexually dimorphic features of meiotic
914 prophase I. Chromosoma. 2019;128(3):199-214.
915 59. Ishiguro KI. Sexually Dimorphic Properties in Meiotic Chromosome. Sex Dev.
916 2023;16(5-6):423-33.
917 60. Turner JMA. Meiotic Silencing in Mammals. Annual Review of Genetics, Vol 49.
918 2015;49:395-412.
919 61. MacQueen AJ, Hochwagen A. Checkpoint mechanisms: the puppet masters of meiotic
920 prophase. Trends Cell Biol. 2011;21(7):393-400.
921 62. Namekawa SH, Park PJ, Zhang LF, Shima JE, McCarrey JR, Griswold MD, et al.
922 Postmeiotic sex chromatin in the male germline of mice. Curr Biol. 2006;16(7):660-7.

63. Müller S, Almouzni G. A network of players in H3 histone variant deposition and maintenance at centromeres. Bba-Gene Regul Mech. 2014;1839(3):241-50.
64. Câmara AS, Schubert V, Mascher M, Houben A. A simple model explains the cell cycle-dependent assembly of centromeric nucleosomes in holocentric species. Nucleic Acids Res. 2021;49(16):9053-65.
65. Fellmeth JE, McKim KS. Meiotic CENP-C is a shepherd: bridging the space between the centromere and the kinetochore in time and space. Essays Biochem. 2020;64(2):251-61.
66. Hockens C, Lorenzi H, Wang TT, Lei EP, Rosin LF. Chromosome segregation during spermatogenesis occurs through a unique center-kinetic mechanism in holocentric moth species. Plos Genet. 2024;20(6).
67. Xiang YB, Tsuchiya D, Yu ZL, Zhao X, McKinney S, Unruh J, et al. Multiple reorganizations of the lateral elements of the synaptonemal complex facilitate homolog segregation in Bombyx mori oocytes. Curr Biol. 2024;34(2).
68. Ma W, Schubert V, Martis MM, Hause G, Liu ZJ, Shen Y, et al. The distribution of α-kleisin during meiosis in the holocentromeric plant Luzula elegans. Chromosome Res. 2016;24(3):393-405.
69. Paull TT, Rogakou EP, Yamazaki V, Kirchgessner CU, Gellert M, Bonner WM. A critical role for histone H2AX in recruitment of repair factors to nuclear foci after DNA damage. Curr Biol. 2000;10(15):886-95.
70. Redon C, Pilch D, Rogakou E, Sedelnikova O, Newrock K, Bonner W. Histone H2A variants H2AX and H2AZ. Curr Opin Genet Dev. 2002;12(2):162-9.
71. Calvente A, Viera A, Parra MT, de la Fuente R, Suja JA, Page J, et al. Dynamics of cohesin subunits in grasshopper meiotic divisions. Chromosoma. 2013;122(1-2):77-91.
72. Talbert PB, Henikoff S. What makes a centromere? Exp Cell Res. 2020;389(2).
73. Page J, Suja JA, Santos JL, Rufas JS. Squash procedure for protein immunolocalization in meiotic cells. Chromosome Res. 1998;6(8):639-42.
74. Schindelin J, Arganda-Carreras I, Frise E, Kaynig V, Longair M, Pietzsch T, et al. Fiji: an open-source platform for biological-image analysis. Nat Methods. 2012;9(7):676-82.
75. Nosil P, Gompert Z, Funk DJ. Divergent dynamics of sexual and habitat isolation at the transition between stick insect populations and species. Nat Commun. 2024;15(1).